Stem Cell Reports
Article

ISSCR

OPEN ACCESS

Satellite glia of the adult dorsal root ganglia harbor stem cells that yield glia under physiological conditions and neurons in response to injury

Madlyne Maniglier,[1] Marie Vidal,[1,2] Corinne Bachelin,[1] Cyrille Deboux,[1] Jérémy Chazot,[1] Beatriz Garcia-Diaz,[1,3,*] and Anne Baron-Van Evercooren[1,*]

[1]Sorbonne Université, Institut du Cerveau - Paris Brain Institute-ICM, INSERM, CNRS, AP-HP, Hôpital Pitié-Salpêtrière, 75013 Paris, France
[2]Berlin Institute for Medical Systems Biology, Max Delbrück Center for Molecular Medicine in the Helmholtz Association, 10115 Berlin, Germany
[3]Instituto de Investigación Biomédica de Málaga (IBIMA)-Plataforma Bionand, Malaga, Spain
*Correspondence: beatriz.garcia@ibima.eu (B.G.-D.), anne.baron@upmc.fr (A.B.-V.E.)
https://doi.org/10.1016/j.stemcr.2022.10.002

SUMMARY

The presence of putative stem/progenitor cells has been suggested in adult peripheral nervous system (PNS) tissue, including the dorsal root ganglion (DRG). To date, their identification and fate in pathophysiological conditions have not been addressed. Combining multiple *in vitro* and *in vivo* approaches, we identified the presence of stem cells in the adult DRG satellite glial population, and progenitors were present in the DRGs and sciatic nerve. Cell-specific transgenic mouse lines highlighted the proliferative potential of DRG stem cells and progenitors *in vitro*. DRG stem cells had gliogenic and neurogenic potentials, whereas progenitors were essentially gliogenic. Lineage tracing showed that, under physiological conditions, adult DRG stem cells maintained DRG homeostasis by supplying satellite glia. Under pathological conditions, adult DRG stem cells replaced DRG neurons lost to injury in addition of renewing the satellite glial pool. These novel findings open new avenues for development of therapeutic strategies targeting DRG stem cells for PNS disorders.

INTRODUCTION

The adult dorsal root ganglion (DRG) harbors cell bodies of sensory neurons that discriminate a large number of sensory stimuli because of a high degree of morphological and functional diversity (Usoskin et al., 2015). Adult DRG neurons are metabolically and physically supported by two types of glia. First, satellite glial cells (SGCs) extend thin processes around each neuronal body to form an envelope and provide a unique environment of neuroglial communication that regulates neuronal activity (Hanani, 2005; Pannese, 1981). Second, the well-known myelinating and non-myelinating Schwann cells support axons along the peripheral nerve. Macrophages, fibroblasts, and perivascular structures formed by endothelial cells and pericytes also contribute to DRG homeostasis.

Most adult DRG cells are neural crest cell derivatives that migrate extensively to their destination during development. However, whether undifferentiated stem or progenitor cells persist in the adult DRG is still a matter of controversy. Few studies support the possibility that the number of DRG sensory neurons increases progressively during life (Devor and Govrin-Lippmann, 1985), and others refute this hypothesis (La Forte et al., 1991; Pover et al., 1994). An average of 20%–50% of sensory DRG neurons die in response to axotomy (Groves et al., 2003) or capsaicin injection (Czaja et al., 2008). The total number of neurons recovers to normal levels over time in injured DRG of juvenile rats. Injection of bromodeoxyuridine (BrdU) combined with stereological quantification in injured rats revealed newly born cells comprising glial cells and a few neurons (Gallaher et al., 2010, 2014), suggesting, but not proving, replacement of adult DRG cells lost to disease by newly born ones.

The stemness potential (Snippert and Clevers, 2011) of adult DRG was also assessed *in vitro* based on the sphere forming capacity of explants (Li et al., 2007; Namaka et al., 2001). Cells emerging from explanted tissues have been shown to proliferate and form multipotent spheres giving rise to neurons, glial cells, and myofibroblasts. Adult DRG multipotency also occurs *in vivo* and is strongly modulated by environmental cues, with DRG sphere-forming cells giving rise to perivascular pericytes after transplantation in the murine developing brain but myelin-forming Schwann cells when grafted in demyelinated adult spinal cord (Vidal et al., 2015). Fate mapping studies using P0-Cre and Wnt1-Cre/floxed EGFP have demonstrated that the *in vitro* DRG stem cell (SC) properties belong essentially to the PNS neural crest-derived fraction (Nagoshi et al., 2008).

Although these studies provided some hints about the presence of adult DRG neurogenesis, the experiments were not conclusive because they were performed with mixed or global adult DRG populations. Late progenitors derived from multiple neural crest cells (Sabourin et al., 2009) or SCs (Vidal et al., 2015) that persist in the DRG through adulthood could have been the source of these newly formed neurons (Farel, 2003). Because of technical limitations, clear identification of the putative DRG SCs and their stemness behavior under physiological and pathological conditions was never established. This fundamental biological question is crucial at a clinical level

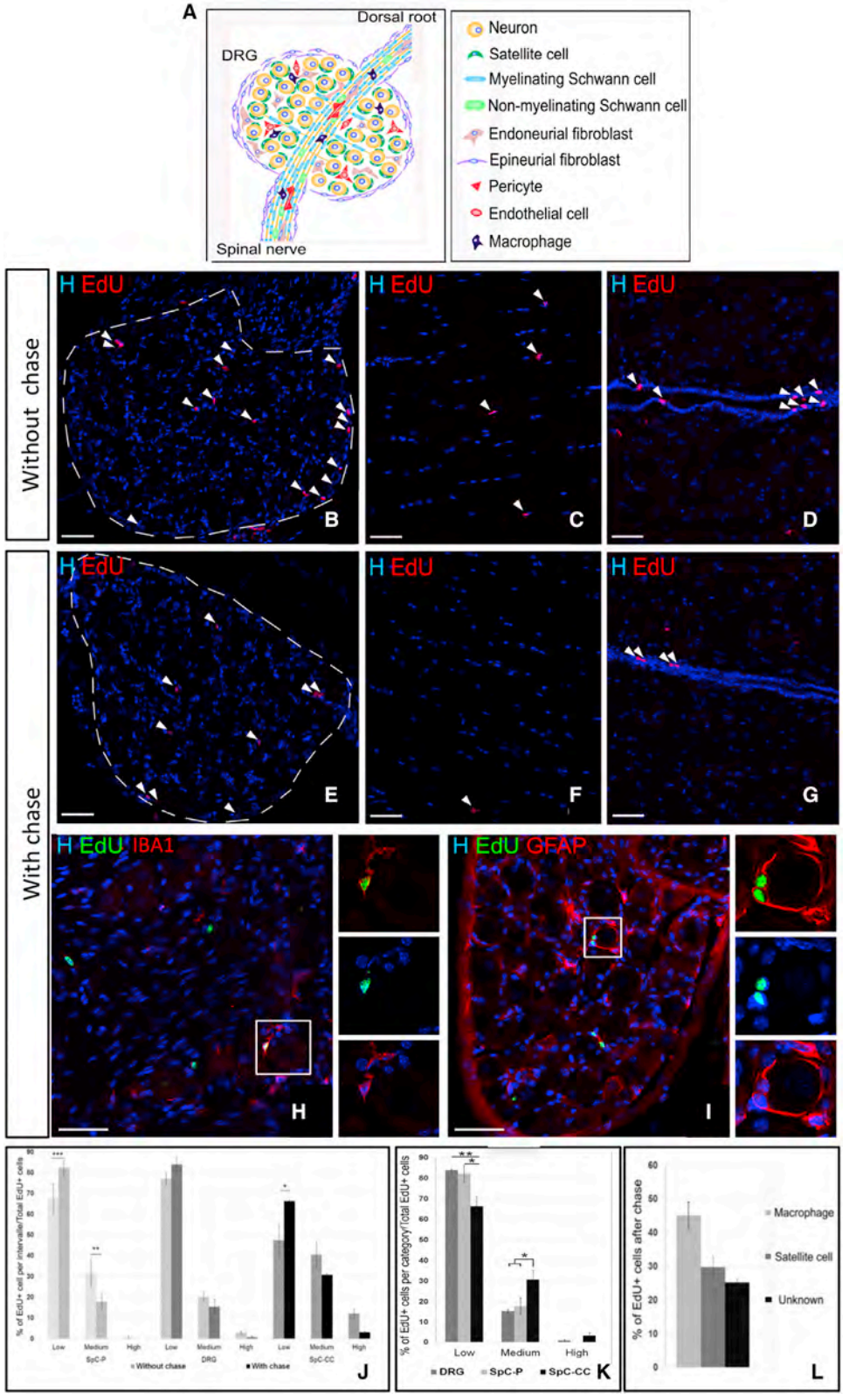

(legend on next page)

because these presumed DRG SCs could be ideal targets to modulate in PNS disorders such as peripheral neuropathies.

To resolve these unanswered questions, we combined multiple *in vivo* and *in vitro* approaches and SC-specific transgenic tools to identify, purify, and characterize the most putative DRG SCs *in vitro* and study their fate under physiological and pathological conditions *in vivo*. Taking the adult spinal cord as reference to validate our transgenic tools, we report that the adult DRG contains SCs and progenitor cells. Adult DRG SCs are a subpopulation of SGCs, which have the capacity to generate neurons and glia *in vitro* and *in vivo* in response to injury.

RESULTS

The adult mouse DRG contains slowly proliferating cells

Because the adult DRG is composed of multiple cell populations (Figure 1A), we first considered that each DRG cell type could constitute the putative DRG SCs. To eliminate some candidates, we used the EdU long-label retention assay to detect the presence of quiescent or slowly proliferating SCs in the adult DRG (Taupin, 2007) and discriminate them from the more proliferative progenitor cells. Spinal cords of the same animals were used as controls to validate our tools because they harbor neural SCs localized in the central canal wall (Meletis et al., 2008) and glial progenitors in the parenchyma (Horner et al., 2000) and referred to CNS SC.

The 5-Ethynyl-2′-deoxyuridine (EdU) incorporation assay without (Figures 1B–1D) or with 1-month chase (Figures 1E–1G) identified the presence of proliferating cells in the adult DRG (Figures 1B–1E). Their low number with chase (<1%) in 4-month-old mice was consistent with the relative quiescence of SCs. This assay validated the presence of EdU^+ progenitor cells in the spinal cord parenchyma without chase only (Figures 1C and 1F) and EdU^+ SCs in the central canal wall (Figures 1D and 1G).

We assumed that the more cells divide rapidly (i.e., progenitors), the more their EdU content is diluted. The EdU dilution effect was assessed by comparing EdU levels without and with chase for each tissue (DRG and spinal cord parenchyma or central canal) based on the percentage of BrdU staining overlap with Hoechst (EdU^{+low} < 30%, $EdU^{+medium}$ < 66%, EdU^{+high} > 66%). Without chase, the 3 regions contained a high percentage of EdU $+^{low}$ cells and a small percentage of $EdU^{+medium}$ and EdU^{+high} cells (Figure 1J, light versus dark gray columns). Although, after the chase, the amount of EdU^{+low} cells in the DRG and the parenchymal spinal cord increased slightly, EdU^{+high} cells were detected in the DRG and the spinal cord central canal wall only (Figures 1J and 1K). Values of the EdU dilution pattern of DRG cells were comprised between the spinal cord parenchymal progenitors and the spinal cord central canal SCs, suggesting that DRG SCs proliferate at a different rate than spinal cord SCs or that the DRG contains multiple populations of proliferating cells.

Without excluding the first possibility, we validated the second one, characterizing the EdU^+ populations in these different tissues. The marker cell specificity according to tissues type is listed in Table S1. In the spinal cord central canal, EdU^+ cells were $IBA1^+$ microglia/macrophages and Glial Fibrilary Acidic $Protein^+$ ($GFAP^+$) SCs (Figures S1A–S1C), and in the spinal cord parenchyma, EdU^+ cells were IBA1+ microglia and $NG2^+$ oligodendrocyte progenitors but not $GFAP^+$ astrocytes (Figures S1D–S1F). In the DRG, EdU^+ cells were subdivided into at least 3 distinct populations comprising $IBA1^+$ microglia/macrophages (45% + 4%; Figures 1H and 1L), $GFAP^+$ perineuronal SGCs (30% ± 3%; Figures 1I and 1L), and an unidentified population (25% ± 3%; Figure 1L). This population included possibly pericytes, fibroblasts, endothelial cells, non-myelinating Schwann cells, or SGCs that did not express GFAP, given that there is no specific and selective marker for the entire SGC population Therefore, we define SGCs as DRG cells that are labeled with GFAP/SOX10 and display morphological features consistent with perineuronal ensheathment.

Even though, at this point, several DRG cell types remained SC candidates, some could be excluded *de facto* from the list. These comprised myelinating Schwann cells and neurons that do not proliferate and epineurial fibroblasts localized at the DRG periphery that proliferate too rapidly to retain EdU during the chase period (compare

Figure 1. *In Situ* characterization of slowly proliferating cells in the adult DRG

(A) Schematic of the different adult DRG cell types.

(B–I) Immunodetection of EdU^+ cells (arrows) without or with chase in the DRG (B, E, H, and I), spinal cord parenchyma (C and F), and spinal cord central canal (D and G).

(H and I) DRG cells immunolabeled for EdU, IBA1, or GFAP.

(J and K) Comparative EdU dilution pattern before and after chase (J) and between the three different regions after chase (K).

(L) Proportion of the different EdU^+ cell types after chase.

Scale bars, 50 μm. Boxed areas are enlarged in the right panels. Data are shown as mean ± SEM (n = 3–4). two-way ANOVA and multiple comparisons: Dunnett's test (J and K), Tukey's test (L); **p < 0.01, *p < 0.05. See also Figure S1.

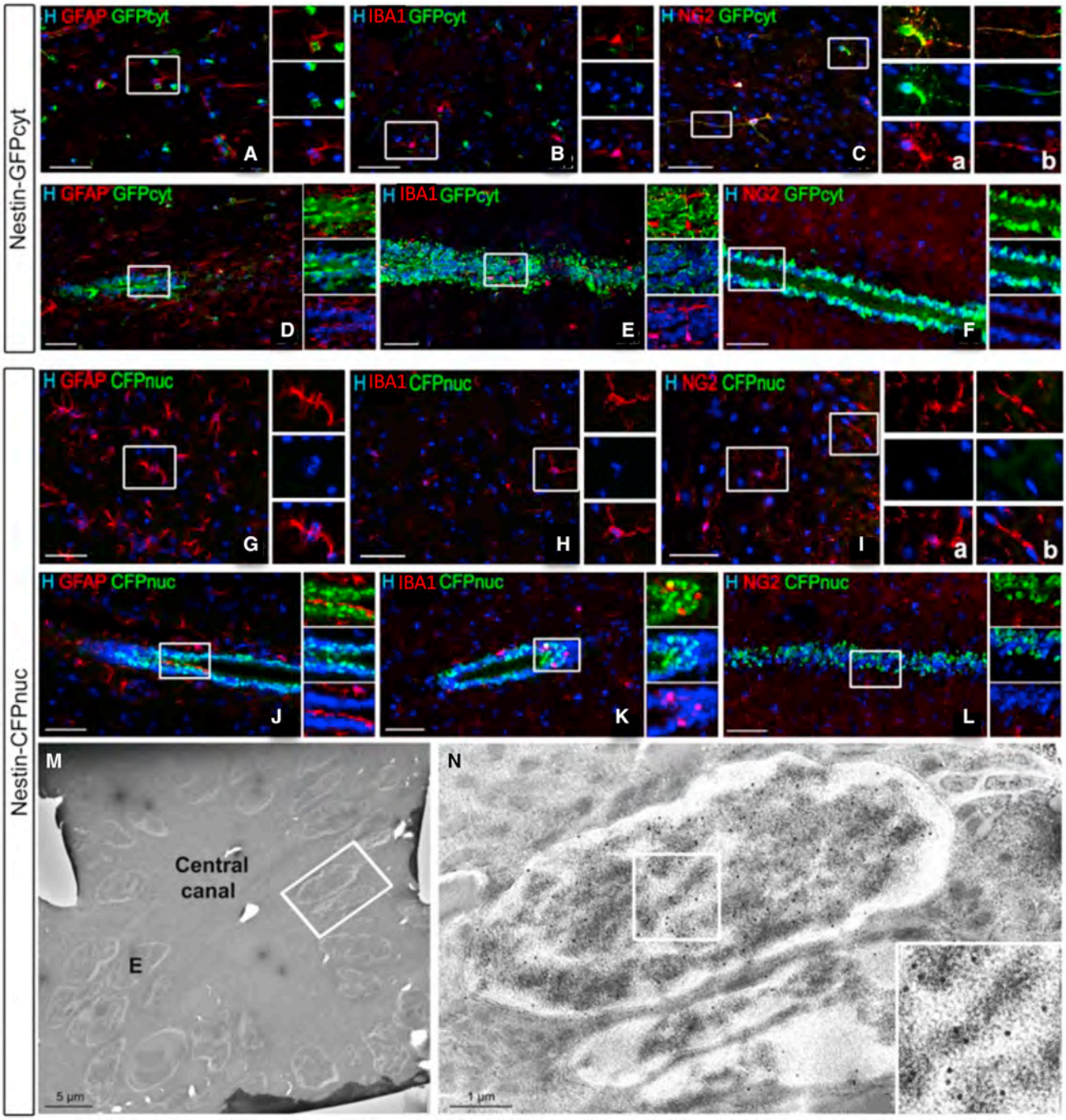

Figure 2. Characterization of transgene expression in Nestin-GFPcyt and Nestin-CFPnuc transgenic spinal cords

(A–L) Double immunohistochemistry for GFP (A–F) and CFP (G–L) and cell-specific markers in the spinal cord parenchyma (A–C and G–I) or central canal (D–F and J–L): $GFAP^+$ astrocytes (A, D, G, and J), $IBA1^+$ microglia (B, E, H, and K), and $NG2^+$ oligodendrocyte progenitors (C, inset a, and I, inset a) or pericytes (C, inset b; I, inset b; and L). Boxed areas are enlarged in the right panels.

(M and N) Visualization by EM of immunogold-labeled ependymal cell nuclei in the Nestin-CFPnuc spinal cord. E, ependymal cell.

Scale bars: 50 μm (A–L), 5 μm (M and N), and 1 μm (E2).

Figures 1B and 1E). Because of the low proportion of EdU^{+high} cells and the lack of tools specifically discriminating each DRG cell type from potential immature cells, identification and characterization of the putative DRG SCs remained difficult using solely the EdU incorporation assay.

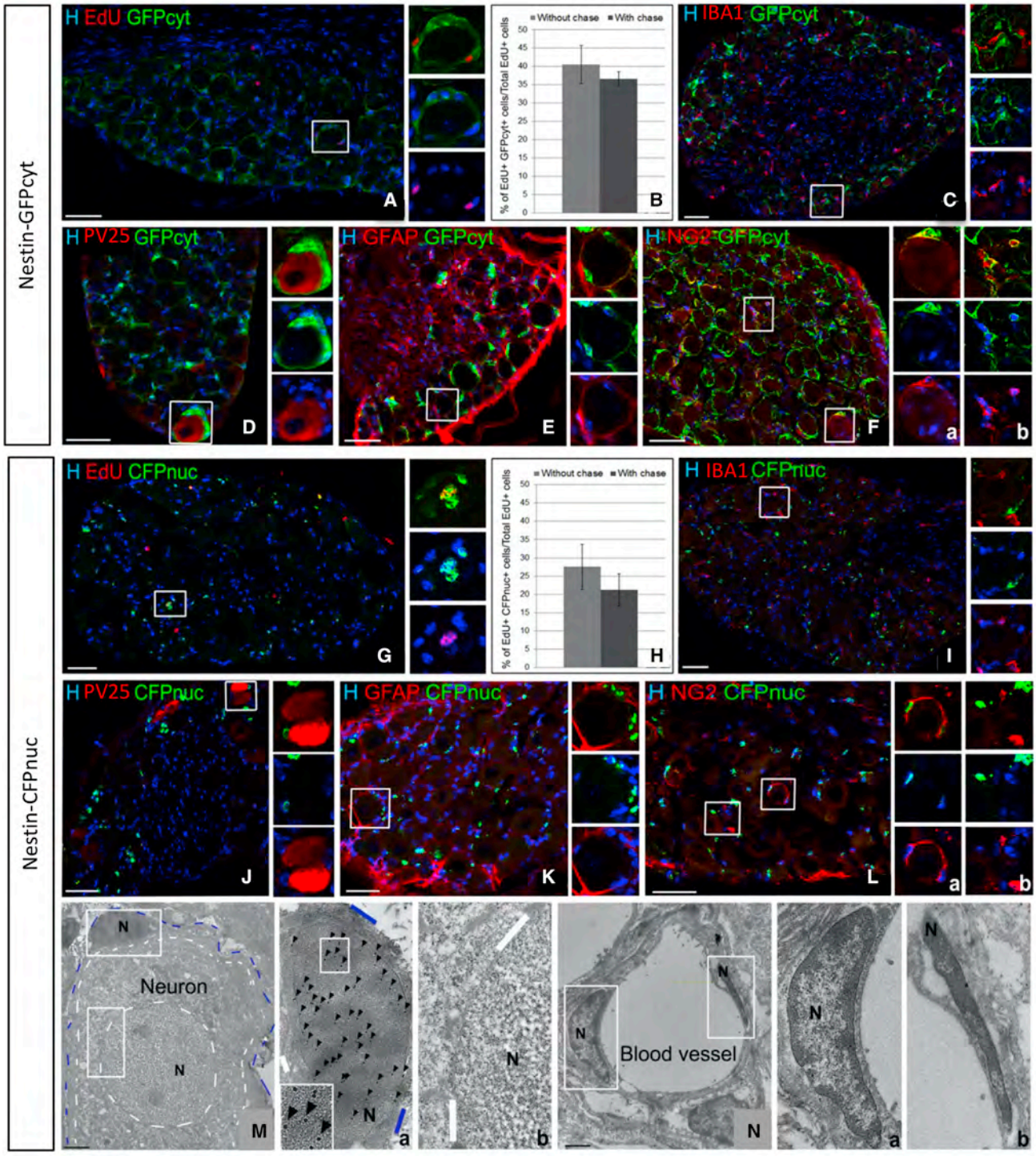

Figure 3. Characterization of GFPcyt$^+$ and CFPnuc$^+$ cells in the adult DRGs of Nestin-GFPcyt and Nestin-CFPnuc reporter mice

(A–L) Immunodetection and quantification of EdU$^+$ cells in Nestin-GFPcyt (A–F) or Nestin-CFPnuc (G–L) mice.

(C–F and I–L) Double immunohistochemistry to reveal GFP (C–F) or CFP (I–L) and IBA1$^+$ macrophages (C and I), PV25$^+$ proprioceptive neurons (D and J), GFAP$^+$ glial cells (E and K), and NG2$^+$ SGCs (F, inset a, and L, inset a) or pericytes (F, inset b, and L, inset b).

(legend continued on next page)

Validation of the Nestin-GFPcyt and Nestin-CFPnuc transgenic lines to identify SCs and progenitor cells in the adult spinal cord

Nestin is a marker of CNS SCs. To clearly identify the putative DRG SCs *in situ* and isolate them *in vitro*, we explored use of Nestin-Green Fluorescent Protein (GFP) cytoplasmic (GFPcyt) (Mignone et al., 2004) and Nestin-Constitutively Fluorescent Protein (CFP) nuclear (CFPnuc) (Encinas et al., 2006) transgenic mice. The Nestin-GFP line encompasses stem/early progenitors and late progenitor populations in the brain (Mignone et al., 2004), and the Nestin-CFP line labels stem/early progenitors only (Encinas et al., 2006).

First we validated transgene expression in the adult spinal cord as a positive control in the same tissue section of connected DRG. Three populations of GFP$^+$ cells were detected in the Nestin-GFPcyt spinal cord (Figure 2). These included parenchymal GFAP$^+$ astrocytes (Figure 2A) and parenchymal NG2$^+$ oligodendrocyte progenitors and pericytes (Figure 2C) in addition to ependyma-associated GFAP$^+$ SCs of the central canal (Figure 2D). Although some IBA1$^+$ microglia/macrophages were EdU$^+$ in the previous chase experiment, they were not GFPcyt$^+$ in the spinal cord (Figures 2B and 2E).

In contrast, CFPnuc expression in the Nestin-CFPnuc$^+$ transgenic mouse line was restricted to the ependyma-associated GFAP$^+$ SC population (Figure 2J) but excluded from the parenchymal astrocyte, microglia/macrophage, and oligodendrocyte progenitor populations (Figures 2G and 2I). These results were confirmed by immunogold electron microscopy for CFPnuc based on the presence of immunogold particles restricted to the nucleus of ependymal ciliated cells of the central canal (Figures 2M and 2N). These immunofluorescent and immunogold electron microscopy observations in the adult spinal cord validate those in the adult brain for late progenitors in GFP mice (Mignone et al., 2004) but SCs/early progenitors in CFP mice (Encinas et al., 2006).

The Nestin-GFPcyt mouse line labels three distinct cell types in the DRG

Nestin-GFPcyt$^+$ and Nestin-CFPnuc$^+$ cells were also found in the DRG (Figure 3), raising the possibility that the adult DRG contains SCs and progenitor cells. Using the EdU chase assay as above, we defined that some DRG GFPcyt$^+$ (Figure 3A) and CFPnuc$^+$ cells (Figure 3G) were also EdU$^+$. The percentage of EdU$^+$/GFPcyt$^+$ cells over the entire DRG EdU$^+$ population was superior to that of the EdU$^+$/CFPnuc$^+$ population after chase (37% ± 2% versus 21% ± 4%, p = 0.03) (compare Figures 3B and 3H), suggesting that a difference between the two transgenic lines existed in the DRG as well. To validate this hypothesis and identify the putative DRG stem and progenitor cells, we characterized the DRG CFPnuc$^+$ and GFPcyt$^+$ cells by immunohistochemistry.

DRG GFPcyt$^+$ cells were localized around DRG neurons (Figure 3D), a location typical for the previously described neuroglial unit (Hanani, 2005; Milosavljević et al., 2021; Pannese, 1981). The great majority of these perineuronal GFPcyt$^+$ cells expressed the SGC markers GFAP (78% ± 9%; Figure 3E) and SOX10 (47% ± 17%; Figure S2), which label neural crest cells and their derived progeny including SGCs (Britsch et al., 2001), and the oligodendrocyte progenitor marker NG2, also known to be expressed in SGCs (Rezajooi et al., 2004; Figure 3F, inset a). Perineuronal GFPcyt$^+$ cells never expressed IBA1 (Figure 3C) nor the neuronal marker PV25 (Figure 3D). However, not all of the Nestin-GFPcyt$^+$ cells were associated with neurons because some of them were located in the endoneurium. These endoneurial Nestin-GFPcyt$^+$ cells expressed NG2 (Figure 3F, inset b), the endoneurial fibroblast/endothelial marker CD34 (Hirose et al., 2003; Richard et al., 2012; Figure S3B), or the pericyte marker CD13 (Figure S3C), but none expressed the myelinating Schwann cell marker P0 (Figure S3A).

These data indicate that the GFPcyt$^+$ population of the Nestin-GFPcyt adult PNS comprised pericytes and endoneurial fibroblasts in addition to SGCs.

The Nestin-CFPnuc mouse line labels a subpopulation of DRG satellite cells

In contrast, CFPnuc expression in the DRG of Nestin-CFPnuc mice was more restricted than GFPcyt expression, as observed for the spinal cord. Within the DRG, CFPnuc$^+$ were Edu$^+$ (Figure 3G), always surrounding neuronal bodies and expressing SGC markers (GFAP+: 81% ± 2%, Figure 3K; SOX10: 46% ± 7%, Figure S2; NG2: Figure 3L, inset a). However, they never expressed markers of microglia/macrophage (Figure 3I), neuron (Figure 3J), myelinating Schwann cell (Figure S3D), fibroblast/endothelial cell (Figure S3E) or pericyte (Figure S3F). Thus, unlike GFPcyt expression, DRG CFPnuc expression was confined to only one cell type, the SGC. This observation was validated by immunogold labeling of Nestin-CFPnuc DRGs by electron microscopy. Gold particles were limited to the nucleus of cells extending very thin flat processes

(M and N) EM analysis of Nestin-CFPnuc DRGs after CFP immunogold labeling. Gold particles (arrowheads) were detected only in SGC nuclei (M, inset a) and were absent from neuron (M, inset b), pericyte (N, inset a), and endothelial cell (N, inset b) nuclei. Blue and white dotted lines delineate SGCs and neurons, respectively. Boxed areas are enlarged in the right panels. N, nucleus.
Scale bars: 50 μm (A–L) and 2 μm (M and N). Data are shown as mean ± SEM (n = 3), two-way ANOVA. See also Figures S2 and S3.

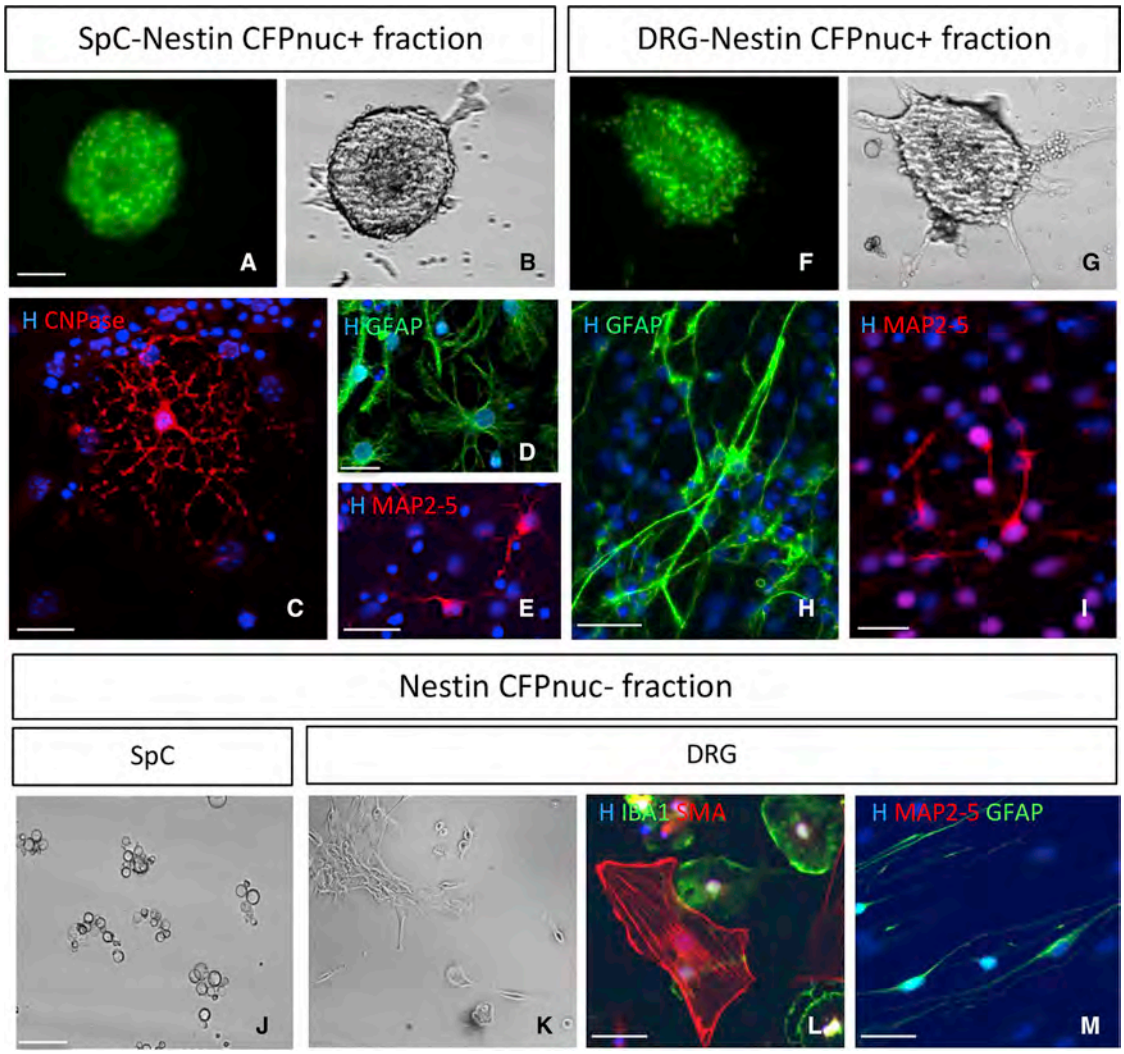

Figure 4. *In vitro* analysis of SC properties of purified Nestin-CFPnuc$^+$ and Nestin-CFPnuc$^-$ cells

(A–G) Ten days after *in vitro* expansion under subclonal conditions (<5 000 cells/mL) in EGF/FGF, FACS-purified adult CFPnuc$^+$ spinal cord cells (SpCs) (A and B) or CFPnuc$^+$ DRG cells (F and G) gave rise to CFP$^+$ spheres.

(C–I) After growth factor removal and adhesion, spinal cord primary spheres differentiated into typical CNPase$^+$ multi-branched oligodendrocytes (C), GFAP$^+$ ramified astrocytes (D), and MAP2–MAP5$^+$ process-extending neurons (E), whereas DRG primary spheres differentiated into GFAP$^+$ bipolar spindle-shaped Schwann cells (H) and MAP2–MAP5$^+$ process-extending neurons (I).

(J and K) Phase illumination shows that, after FACS purification, CFPnuc$^-$ SpCs died over time (J), whereas CFPnuc− DRG cells generated adhering bipolar cells (K).

(L and M) After growth factor removal, CFPnuc− DRG primary spheres differentiated into αSMA$^+$ flat fibroblasts, IBA1$^+$ pancake-shaped microglia/macrophages (L), and GFAP$^+$ spindle-shaped PNS glia but not into MAP2–MAP5$^+$ neurons (M).

Scale bars: 20 μm (A–G, J, and K) and 100 μm (C–E, H, I, L, and M). See also Figure S4.

encasing individual neuronal cell bodies, corresponding, by definition, to SGCs (Figure 3M, inset a). The nuclei of the other DRG cell types, including neurons (Figure 3M, inset b), pericytes, endothelial cells (Figure 3N, insets a and b), myelinating Schwann cells (Figures S3G and S3H), macrophages (Figures S3I and S3J), or fibroblasts (Figures S3K and S3L), were never immunolabeled. When comparing the two lines, the fraction of perineuronal GFAP$^+$ SGCs expressing CFPnuc (50% ± 7%) was reduced compared with those expressing GFPcyt (89% ± 6%).

The present data indicate that putative progenitors and SCs are present in the adult DRG. Although Nestin-GFPcyt mice had identified parenchymal progenitors and perineuronal SCs in the DRGs, the Nestin-CFPnuc mouse line traced only the presumptive DRG SCs with clear features of SGCs.

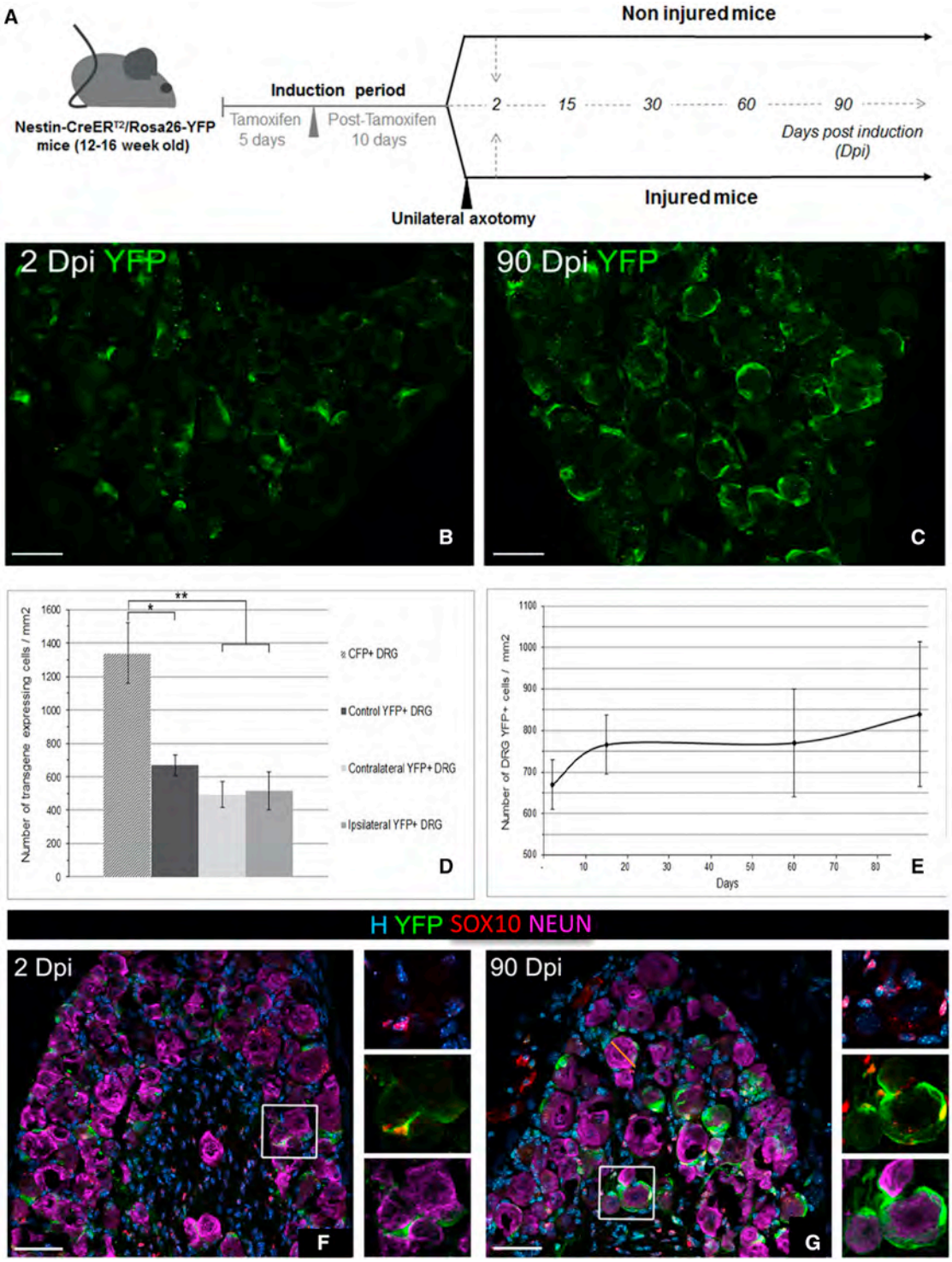

Figure 5. Fate mapping of adult DRG SCs

(A) Schematic representation of tamoxifen induction and temporal analysis of Nestin-CreER^{T2}/Rosa26-YFP mice.

(B and C) Detection of adult DRG-YFP^{+} cells 2 and 90 days after tamoxifen induction (dpi).

(D) Number of DRG transgenic positive cells per square millimeter at 2 dpi in CFPnuc mice and ipsi/contra injured or non-injured mice.

(E) Temporal evolution of the number of DRG-YFP^{+} cells per square millimeter.

(legend continued on next page)

DRG SCs give rise to neurons and glia *in vitro*

Taking advantage of the high specificity of the Nestin-CFPnuc transgenic line, we purified, by fluorescence-activated cell sorting (FACS), the putative DRG SCs to establish their stemness potential *in vitro,* taking the spinal cord as a positive control. After FACS and seeding, all spinal cord and DRG CFPnuc$^+$ viable cells expressed the transgene, validating their successful purification (Figure S4).

First, we obtained proof that the FACS-purified spinal cord CFPnuc$^+$ fraction was the only fraction capable to form free-floating spheres (Figures 4A and 4B), whereas, under the same growth conditions, the spinal cord CFPnuc$^-$ fraction did not generate spheres and died (Figure 4J). After adhesion and growth factor retrieval to induce differentiation, spinal cord CFPnuc$^+$ spheres were tripotent, as described originally (Meletis et al., 2008; Reynolds and Weiss, 1992), differentiating into oligodendrocytes 2′, 3′ Cyclic Nucleotide 3′ Phosphodiesterase$^+$ (CNPase$^+$), astrocytes (GFAP$^+$), and neurons (MAP2–MAP5+; Figures 4C–4E), validating that the Nestin-CFPnuc mouse line identifies CNS SCs.

Next we isolated, by FACS, the Nestin-CFPnuc$^+$ and Nestin-CFPnuc$^-$ fractions from the DRGs. After 10 days under epidermal growth factor (EGF)/fibroblast growth factor (FGF) conditions, cells of the positive fraction were able to proliferate and formed free-floating spheres that maintained Nestin-CFPnuc expression (Figures 4F and 4G). In the absence of EGF/FGF, these CFPnuc$^+$ spheres differentiated, in great majority, into the major DRG constituents, including bipolar Schwann cells (GFAP$^+$), but also into typical neurons (MAP2–MAP5$^+$) with round cell bodies and long processes but never into Smooth Muscle Actin$^+$ (SMA$^+$) flat myofibroblasts (Figures 4H and 4I). The observation of *de novo* neurogenesis and *in vitro* bipotency of the FACS-sorted DRG CFPnuc$^+$ cells reinforced the stemness of the putative DRG SCs. Under proliferation conditions, the DRG CFPnuc$^-$ fraction, unlike the spinal cord CFPnuc$^-$ fraction, generated adhering bipolar cells (Figure 4K) that eventually formed aggregates at later times. Under differentiation conditions, CFPnuc$^-$ cells gave rise to flat fibroblasts or pericytes, microglia/macrophages, and spindle-shaped Schwann cells but never to neurons (Figures 4L and 4M).

Fate mapping of adult DRG SCs highlights their gliogenic potential in physiological condition

We showed that, under healthy conditions, DRG SCs proliferate slowly *in situ* without elucidating the phenotype of their newly born cells. *In vitro*, adult DRG SCs formed bipotent spheres giving rise to neurons and glial cells. Because the "stemness potential" of the DRG SC could have been overestimated *in vitro* (Singec et al., 2006; Snippert and Clevers, 2011), we questioned whether these newly identified cells behaved as *bona fide* SCs *in vivo* and whether they participated in physiological and/or pathological tissue homeostasis. To fate map the progeny of the adult DRG SCs, we crossed the Nestin-CreER^{T2} line with the Rosa26-Yellow Fluorescent Protein (YFP) reporter line (Imayoshi et al., 2006). Nestin-CreER^{T2} activity was induced by daily tamoxifen gavage during 5 days in 3- to 4-month-old Nestin-CreER^{T2}:
Rosa26-YFP mice (Figure 5A). To evaluate the percentage of recombined DRG SCs in Nestin-CreER^{T2}:Rosa26-YFP mice, we compared the density of DRG transgene-expressing cells (number of YFP$^+$ cells per square millimeter) with that of CFPnuc mice. At 2 days post induction (dpi), their number was significantly lower in non-injured (control, 663 ± 60) Nestin-CreER^{T2}:Rosa26-YFP DRGs compared with CFPnuc DRGs (1,340 ± 180), suggesting a YFP recombination efficiency of the DRG SC population of around 44% (Figure 5D).

After a resting period of 10 days to eliminate systemic tamoxifen, the permanently recombined YFP$^+$ cells were analyzed in non-injured animals at different time points after induction under physiological conditions (Figures 5B and 5C). YFP$^+$ cells were never detected in sham-induced animals (oil administration only; data not shown). We next examined the evolution of this YFP$^+$ population by quantifying their number at 2, 15, 60, and 90 dpi (Figure 5E). The DRG-YFP$^+$ cell density (total amount per square millimeter) remained stable over time, but a progressive but not significant increase occurred with time (664 ± 65, 749 ± 87, 755 ± 144, and 821 ± 195 YFP$^+$ cells/mm^2 at 2, 15, 60, and 90 dpi, respectively), suggesting slow proliferation of DRG SCs or frequent turnover of their progeny under healthy endogenous conditions.

YFP$^+$ SGC cells, identified by their perineuronal, small crescent moon-like phenotype and strongly Hoechst-stained nuclei, were easily distinguished from YFP$^+$ DRG neurons, which had large round cell bodies and large faintly Hoechst-stained nuclei. Based on these criteria, all recombined YFP$^+$ cells at 2 dpi were SGCs and not neurons (Figures 5B, 5F, 7A, and 7D). Immunocharacterization at 2 dpi demonstrated that YFP expression was restricted to typical perineuronal SGCs (GFAP$^+$: 92% ± 6%, Figure S5A; SOX10$^+$: 69% ± 11%, Figures 5F and 5G). Recombined

(F and G) Immunodetection of adult DRG-YFP$^+$ cells with SOX10 (glial cells) and NEU-N (neurons) at 2 (F) and 90 dpi (G) in non-injured Nestin-CreER^{T2}/Rosa26-YFP mice. Boxed areas are enlarged in the right panels.

Data are shown as mean ± SEM (n = 3). One-way ANOVA and multiple comparisons: Dunnett's test (D) and Tukey's test (E); $^{**}p < 0.01$, $^{*}p < 0.05$. See also Figure S5.

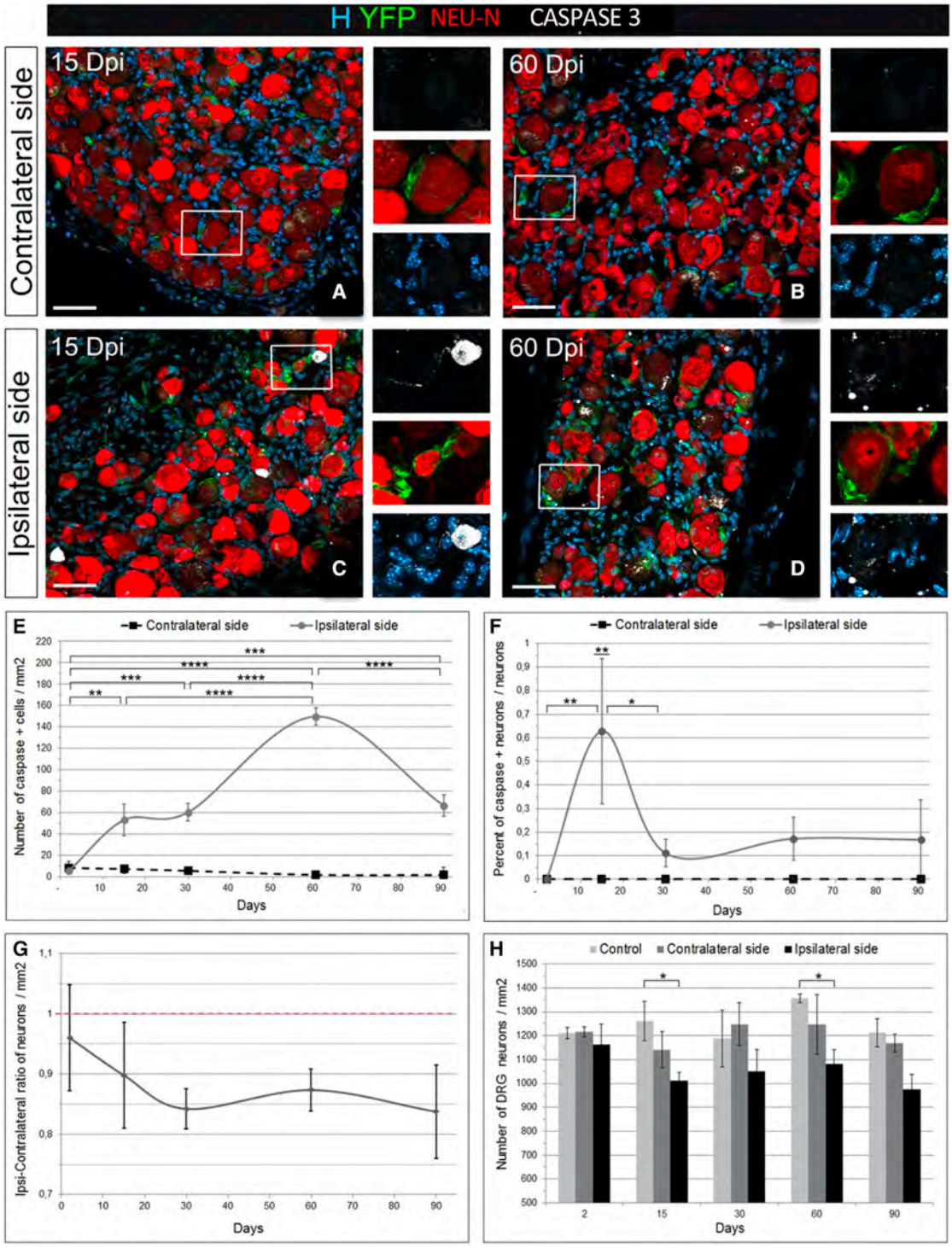

Figure 6. Effect of sciatic nerve axotomy on DRG neurons in Nestin-Cre-ER^{T2}/Rosa26-YFP DRGs

(A–D) Immunohistochemistry for YFP, activated caspase-3, and NEU-N on the DRG contra side or ipsi side at 15 dpi (A and C) and 60 dpi (B and D). Boxed areas are enlarged in the right panels.

(E) Temporal evolution of the density of apoptotic caspase-3$^+$ cells (contra and ipsi sides) after axotomy.

(F) Proportion of apoptotic neurons (caspase-3$^+$) over the total neuronal (NEU-N$^+$) population.

(legend continued on next page)

YFP$^+$ cells never expressed markers of neurons (Neuronal Nuclear Antigen (NEU-N); Figures 5F and 5G) or of other DRG cell types (Figures S5C–S5H), such as macrophages (IBA1), Schwann cells (P0), pericytes (CD13), or endothelial cells/fibroblasts (CD34). Analysis of the YFP$^+$ population phenotype at 90 dpi indicated that, under physiological conditions, the DRG-YFP$^+$ progeny had the unique fate to become SGCs (GFAP$^+$, 89% ± 6%; SOX10$^+$, 67% ± 0.7%) because no cell type other than SGCs expressed YFP (Figures 5G and S5B). These results validate that, under physiological conditions, YFP expression was restricted to a subpopulation of SGCs, DRG SCs, that expressed Nestin, as described for Nestin-CFPnuc mice.

Long-term lineage tracing of adult DRG SCs reveals their glio- and neurogenic potential after PNS injury

To examine the role of DRG SCs under pathological conditions, we challenged their response to nerve injury and questioned their participation in the regenerative process, using the same tracing paradigm as under physiological conditions (Figure 5A). Previous studies indicated that a variety of cellular changes occur in DRGs after sciatic nerve axotomy, including death of neurons and SGCs, followed by proliferation of microglia/macrophages, Schwann cells, and SGCs (Cherkas et al., 2004; Hu and McLachlan, 2002; Pierucci and de Oliveira, 2006). We therefore performed unilateral sciatic nerve axotomy after tamoxifen induction of Nestin-CreER^{T2}/Rosa26-YFP (Nestin-YFP) mice. Tamoxifen induction followed by a 10-day chase prior to axotomy ensured that all recombined DRG cells were DRG SCs and that some did not dedifferentiate or become reactivated cells, such as Schwann cells re-expressing Nestin after injury (Jessen and Mirsky, 2008). Evaluation of the YFP population at 2 dpi showed no significant difference in the density of YFP$^+$ (number per square millimeter) before (663 ± 60) and after injury (ipsilateral side, 515 ± 180; contralateral side, 493 ± 134) (Figure 5D).

Taking the contralateral side of the axotomy as a control, we next temporally assessed the effect of axotomy on cell death in the connected DRGs (L3, L4, and L5) from 2–90 dpi. Caspase-3 immunodetection revealed that cell death was induced in the ipsilateral DRG (Figures 6C and 6D) but not on the contralateral side (Figures 6A and 6B). DRG apoptosis was regulated temporally with a first wave of activated caspase-3$^+$ apoptotic cells appearing at 15 dpi after axotomy in the ipsilateral DRG (significantly higher than at 2 dpi, $p = 0.006$) (Figure 6E) and remaining stable up to 30 dpi, followed by a second wave of apoptosis at 60 dpi in the ipsilateral DRG (significantly higher than at 2 and 15 dpi, $p \leq 0.0001$) and compared with the contralateral side. Although SGC death occurred, in response to sciatic nerve axotomy, as reported previously (McKay Hart et al., 2002; Pierucci and de Oliveira, 2006), we focused our analysis on neuronal death because neurons are the primary target of injury (Pierucci and de Oliveira, 2006). Immunodetection of cleaved caspase-3 together with NEU-N revealed that some of the dying cells were neurons, with a peak of apoptotic neurons at 15 dpi. Although the number of dying neurons was low (0.63% ± 0.3%), neuronal death persisted up to 90 dpi, the latest time point analyzed (Figure 6F). When the numbers of ipsi- versus contralateral neurons per square millimeter were compared (Figure 6G), a slow and progressive loss of neurons was observed in the ipsilateral DRGs up to 30 dpi, with an ipsi-contralateral ratio of 0.85 ± 0.01/mm^2 between 30 and 90 dpi. The total number of neurons per unit area in the ipsilateral DRG was significantly lower than in the control non-injured DRG at 15 ($p = 0.033$) and 60 dpi ($p = 0.018$) (Figure 6H). Thus, unilateral sciatic nerve axotomy had an effect on its connected DRGs by inducing cell death over time, including that of neurons.

SGCs are known to be activated under pathological conditions (Hanani et al., 2002). We therefore tested whether these "activated SGCs" corresponded to DRG SCs. Taking the contralateral side as a control to normalize the recombination bias between animals (Figures 7A–7C versus 7D–7F), we observed a first significant peak of the YFP$^+$ cell ratio at 15 dpi ($p = 0.042$), followed by a second peak at 60 dpi ($p = 0.011$) (Figure 7G). Thus, the ipsilateral YFP$^+$ DRG SCs reacted to PNS injury by increasing cell numbers compared with the contralateral DRG SCs. The YFP$^+$ DRG SC pattern of activation correlated with the waves of DRG cell death (compare Figures 6E and 7G), suggesting their contribution to the DRG regenerative process elicited after injury.

Immunocharacterization of YFP$^+$ cells and their progeny at 2 and 90 dpi in the ipsilateral DRGs of injured animals provided evidence showing that the great majority of the newly generated cells were GFAP$^+$ SGCs (ipsilateral [ipsi] 78% ± 5% and contralateral [contra] 87% ± 6% cells at 2 dpi ipsi 78% ± 6% and contra 72% ± 7% at 90 dpi) (Figure S5) and, to a minor extent, SOX10$^+$ SGCs (ipsi 30% ± 10% and contra 55% ± 15% at 2 dpi and ipsi 44% ± 11% and contra 34% ± 12% at 90 dpi) (Figures 7H and 7J). Large YFP$^+$ cells expressing NEU-N were detected only in the

(G) Ratio of ipsi over contra DRG neuronal density over time.

(H) Histogram of DRG neuron density over time in control non-injured and contra and ipsi injured mice.

Scale bars: 50 μm (A–D). Data are shown as mean ± SEM (n = 3). Two-way ANOVA and multiple comparisons: Tukey's test (E and F), Tukey's test (F), and Dunnett's test (G); ****$p < 0.0001$, ***$p < 0.001$, **$p < 0.01$, *$p < 0.05$.

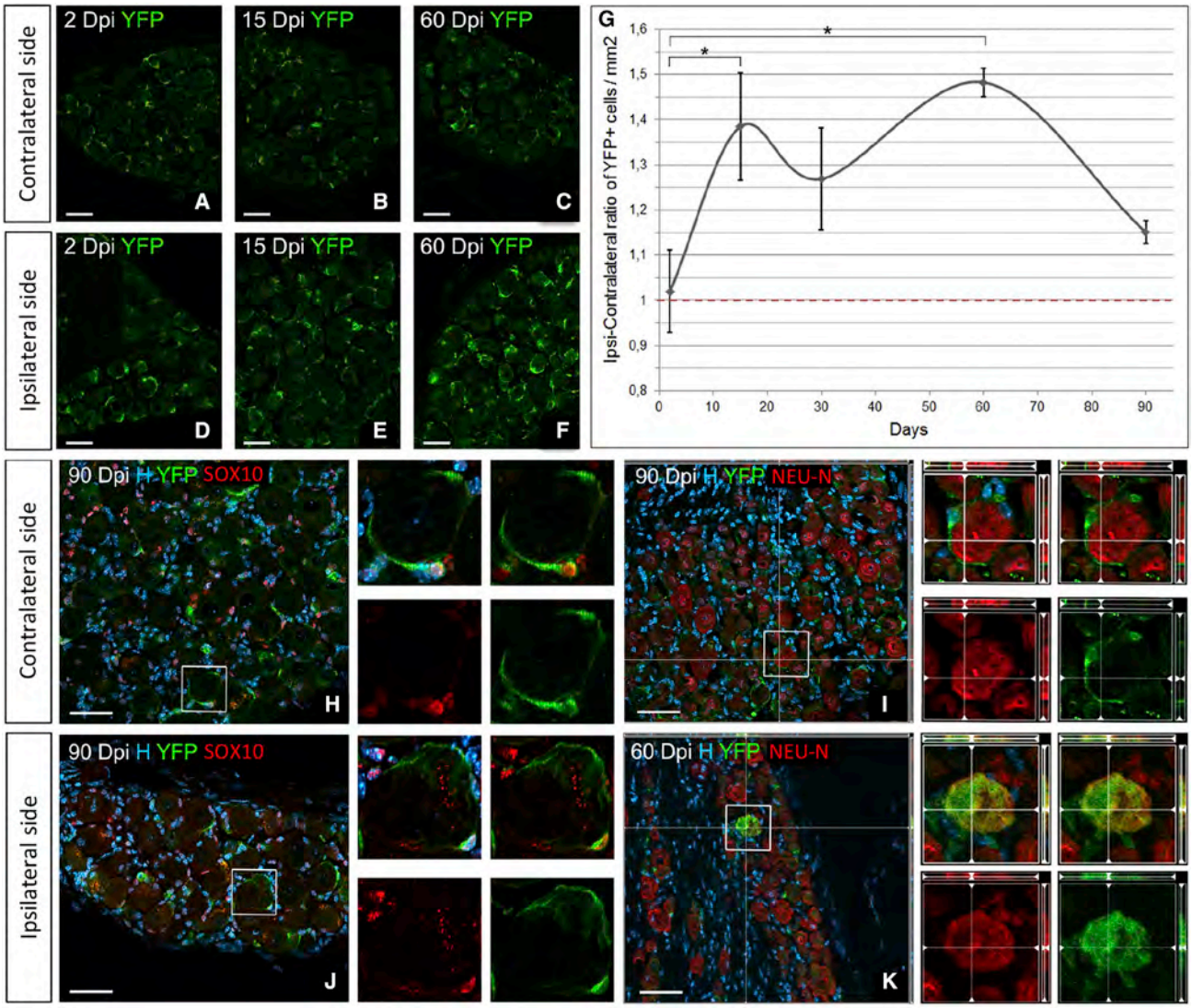

Figure 7. Long-term lineage tracing of adult DRG SCs in axotomized Nestin-CreER^{T2}/Rosa26-YFP animals

(A–F) Immunostaining of contra versus ipsi DRGs for YFP at 2, 15, and 60 days after axotomy.

(G) Temporal evolution of the DRG-YFP$^+$ cell density ratio (ipsi over contra side).

(H–K) Immunocharacterization of adult DRG-YFP$^+$ cells using SOX10 for glial cells (H and J) and NEU-N for neurons (I and K) in the contra or ipsi DRG at 90 dpi.

Scale bar: 50 μm (A–F and H–K). Boxed areas are enlarged in the right panels. In (G), data are shown as mean ± SEM, (n = 3). Two-way ANOVA and multiple-comparisons Dunnett's test; *p < 0.05. See also Figure S6.

ipsilateral DRG of axotomized Nestin-CreER^{T2}/Rosa26-YFP mice (Figures 7I, 7K, and S6G–S6I) mice. Quantification of the percentage of NEU-N$^+$/YFP$^+$ cells over YFP$^+$ cells (ipsi, 0% and 0.24% ± 0.11% at 2 and 90 dpi, respectively; contra, 0% at 2 and 90 dpi) indicated that *in vivo* DRG neurogenesis remains a rare event. The remaining DRG-YFP$^+$ cells tested at 2 and 90 dpi were never microglia/macrophages (IBA1$^+$), myelinating SCs (P0$^+$), pericytes (CD13$^+$), or fibroblasts/endothelial cells (CD34$^+$) (Figures S6A–S6F). Thus, neurogenesis, in addition to gliogenesis, occurred in the adult injured DRG with newly born neurons generated from slowly proliferating Nestin-YFP+ DRG SCs.

DISCUSSION

The observation that dissociated DRG cells can proliferate and form spheres that generate neurons, glia, and myofibroblasts *in vitro* suggests the presence of SCs in adult DRGs (Li et al., 2007; Nagoshi et al., 2008; Namaka et al., 2001; Vidal

et al., 2015). However, their stemness characteristics remained difficult to prove because of technical limitations related to stereological quantification and the lack of specific markers to unambiguously trace the neurogenic population. Therefore, the identity of adult DRG SCs as well as their role under physiological and pathological conditions remained elusive. We used multiple approaches to unambiguously demonstrate the presence of a novel Nestin-expressing cell in the adult DRG SGC compartment. These cells have characteristics of adult SCs *in vitro* and *in vivo*, generating new SGCs under physiological conditions but neurons in addition to SGCs, when required, to replace neurons lost to injury.

Progenitors and SCs are present in the adult mouse DRG

We took advantage of two Nestin reporter mice to uncover the identity of the putative DRG SC candidate. Because of the more restricted expression of the Nestin-CFPnuc line, which labels CNS SCs/early progenitors in the spinal cord and a subpopulation of SGC in the DRG, we were able to isolate and study the stemness potential of the DRG CFPnuc$^+$ fraction. Their unique *in situ* perineuronal location and co-expression of CFP with cell markers such as GFAP, SOX10, and NG2 and EdU incorporation allowed their unambiguous identification as SGCs. In culture, these DRG CFPnuc$^+$ cells were able to form bipotent spheres. In the absence of growth factors and adhesive conditions, CFPnuc$^+$ cells differentiated into neurons and spindle-shaped glial cells. However, in contrast to previous *in vitro* studies using whole DRG preparations (Li et al., 2007; Nagoshi et al., 2008; Vidal et al., 2015), the DRG CFPnuc$^+$ fraction never generated myofibroblasts. Thus, we formulated the hypothesis that, in addition to SCs, the adult DRG contains progenitors, whose identity remains to be unraveled.

The EdU incorporation assay in non-injured wild-type mice allowed us to identify the presence of multiple proliferating cell types in the DRG. We found EdU$^+$ cells with a typical SGC morphology in addition to other EdU$^+$ PNS cell types, such as the slowly proliferating resident macrophages (Müller et al., 2010), pericytes, and a few fibroblasts. This is in contrast to a previous report stating that SGCs are the only slowly proliferating cells of the DRG under physiological conditions (Gallaher et al., 2014). It also highlights that the EdU incorporation assay alone is not sufficient to identify a putative SC without avoiding detection of other misleading candidates. However, use of this assay reduced the number of potential candidates under physiological conditions because myelinating Schwann cells and endothelial cells did not incorporate EdU.

We also found that not all PNS and CNS EdU$^+$ were GFPcyt$^+$ or CFPnuc$^+$. These cells could have been the differentiated progeny of GFPcyt$^+$ or CFPnuc$^+$ cells that lost Nestin expression during the differentiation process. Alternatively, these EdU$^+$/Nestin$^-$ cells could correspond to a cell type that has a physiological turnover (EdU$^+$) without stem or progenitor properties (GFP$^+$ or CFP$^+$), as observed for the PNS/CNS-resident immune cells (Müller et al., 2010). These observations stress the necessity to use multiple transgenic tools combined with *in situ* and *in vitro* characterization to carefully and correctly separate progenitors from SC populations. Because of this meticulous analysis, the present study is the first to clearly identify and characterize SCs and progenitors in the adult DRG. Adult sciatic nerves were analyzed in parallel to the DRG and spinal cord assays. Although rare Edu$^+$ cells were present in this tissue, CFPnuc$^+$ cells were never detected in adult sciatic nerves of Nestin-CFPnuc mice when analyzed *in situ*. Although sciatic nerves generated spheres with time in culture, as demonstrated previously (Takagi et al., 2011), they never generated neurons *in vitro*. These combined *in situ* and *in vitro* observations infer that adult sciatic nerves do not harbor SCs but growth-responsive cells, including macrophages, progenitors, and cells like Schwann cells, that have the capacity to dedifferentiate and proliferate (Mirsky et al., 2008).

DRG SCs have gliogenic and neurogenic fates, depending on the environmental context

Using genetic fate mapping, we demonstrate that adult DRG SC are responsible for DRG gliogenesis and sustain an important turnover of the mature SGC population under physiological conditions. The proliferation capacity attributed previously to SGCs reflects, in fact, a cell-specific characteristic restricted to a subpopulation of SGCs, the Nestin-YFP$^+$ subpopulation. Based on the Edu-CFPnuc assay, only a low percentage of CFPnuc$^+$ DRG SCs (20%) over the total EdU$^+$ population (1.77%) proliferated at a slow rate under physiological conditions (Figures 1D and 3H). The results obtained with the Nestin-CreER line under physiological conditions indicated that, as in the CFPnuc line, the recombined YFP$^+$ cells correspond strictly to a subpopulation of SGCs, with numbers remaining stable over time (Figure 5E). This suggests a homeostatic equilibrium between slow YFP$^+$ SC proliferation and the slow death of their mature SGC-YFP$^+$ progeny to ensure maintenance of the SGC population throughout adulthood.

Proliferation of Nestin-Cre-YFP$^+$ cells increased up to 2 months after injury without reaching a normal plateau, suggesting concomitant DRG SC reactivation and neuronal loss. Characterization of the activated DRG SC progeny in this injury context confirmed the SGC gliogenic potential and neurogenic potential under pathological conditions. The function of mature SGCs under

pathophysiological conditions and their major involvement in neuroprotection of DRG neurons has been highlighted previously (Hanani and Spray, 2020). SGC accomplish re-uptake of neuroactive substances or peripheral toxins, making them more susceptible to death than other DRG cell types (Schaeffer et al., 2010) Thus under pathophysiological conditions, adult DRG SCs may have a dual role. First, they play a crucial role in maintaining the level of mature SGCs, ensuring neuronal survival throughout life. Second, they generate neurons in addition to their glial progeny to refuel the pool of neurons (and glia) lost to axotomy. Although significant, neurogenesis remained a minor event compared with gliogenesis. The cell fate plasticity of DRG SCs is similar in many aspects to the glial SOX10^{+} SCs of the enteric nervous system, which have gliogenic potential under physiological conditions but give rise to neurons after enteric neuronal loss (Laranjeira et al., 2011).

In contrast to CNS SCs, which are restricted to specific brain and spinal cord compartments, DRG SCs seem to be dispersed in their entire tissue to quickly sense environmental changes and efficiently renew the SGC pool of the DRG neuron-glia unit (one neuron and its SGCs). Similar SCs could exist in other PNS tissues, where they mainly generate glia under physiological conditions without being confined to specific SC niches. This sensitivity to environmental modifications may endow these PNS SCs with an improved capacity to respond and adapt to injury and, therefore, contribute to the more efficient regenerative properties of the PNS compared with the CNS.

Conclusion

Although several studies have proposed the presence of DRG SCs, none considered them a distinct SGC population. Their existence, activation, and involvement in glial/neuronal renewal under pathophysiological conditions open a new field of research, especially in neuropathic studies. The "activated" SGC seems to be an entity shared by various peripheral neuropathies caused by chemotherapy (Warwick and Hanani, 2013), injury (Donegan et al., 2013), viruses, and heredity (Sghirlanzoni et al., 2005) and could contribute to the genesis and maintenance of other SGCs (Hanani, 2012) and renewal of neurons. New transgenic models combined with molecular/transcriptomics analysis should provide the ability to further study the contribution and intracellular regulation of DRG SCs under physiological and pathophysiological conditions. These DRG SCs could be pharmacological targets to treat peripheral neuropathies and possibly CNS disorders providing a source of PNS glia known to invade the CNS in response to demyelinating or traumatic conditions (Garcia-Diaz et al., 2019).

EXPERIMENTAL PROCEDURES

Animals

Nestin-CFPnuc (Encinas et al., 2006), Nestin-GFPcyt (Mignone et al., 2004), Nestin Cre ERT2 (Imayoshi et al., 2006), and Rosa26-YFP lines were bred and housed under standard conditions, and experiments were performed according to European Community guidelines (see supplemental information).

EdU pulse-chase assay

EdU (catalog number C35002, Invitrogen) dissolved in PBS (8.33 mg/mL) was administered by intraperitoneal injection at a dose of 75 mg/kg every 12 h during 8 days in 3-month-old wild-type or transgenic (Nestin-CFPnuc or Nestin-GFPcyt) mice (n = 12). Half of the injected mice were sacrificed 12 h after the last injection, and the others were killed after 1 month of chase. DRGs, sciatic nerves, and spinal cords were prepared as described below.

Cre induction

Three to four-month-old double-transgenic mice, Nestin-CreERT2 × Rosa-YFP, received a dose of tamoxifen dissolved in corn oil (30 mg/mL, Sigma, catalog number T5648) by oral administration (210 mg/kg) during 5 days.

Sciatic nerve axotomy

After a resting period of 10 days, tamoxifen-induced animals were anesthetized. In half of the group, the right sciatic nerve was exposed mid-thigh and cut. Injured or non-injured induced mice (n = 3–5 per time point and per group) were sacrificed at different dpi. For detailed information, see supplemental experimental procedures.

Tissue processing for fluorescence immunohistochemistry

DRGs, sciatic nerves, and spinal cords from 4-month-old Nestin-CFPnuc and Nestin-GFPcyt mice (n = 3–4 per line and experimental group) were sacrificed by overanesthesia (Ketamin-Rompan) and perfused *trans*-cardially with a solution of 4% paraformaldehyde (PFA) in phosphate-buffered saline (PBS) 1× before tissue collection and freezing. For detailed information, see supplemental experimental procedures.

Tissue processing for immunogold electron microscopy

Four-month-old Nestin-CFP (n = 5) mice were sacrificed by overanesthesia (Ketamin-Rompan) and *trans*-cardially perfused with 4% PFA in PBS (0.1 M). DRGs and spinal cords were post fixed 1 h in 4% PFA and 0.3% glutaraldehyde (Sigma-Aldrich) and processed for electron microscopy (EM). After sectioning and immunogold staining, ultra-thin sections were examined by transmission electron microscope. For detailed information, see supplemental experimental procedures.

Adult DRG and spinal cord cultures

Isolation

Transgenic 3- to 4-month-old mice were euthanized to collect spinal cords and DRGs, and processed for dissociation. Cells from the two tissues were purified by FACS based on their endogenous expression of CFPnuc and GFPcyt (n = 6 independent replicates/transgenic line). For expansion, cells sorted by FACS were seeded at semi-clonal concentration and cultured in suspension as spheres *in vitro*. For differentiation, 15- 20- day primary spheres were induced to adhere and cultured without growth factor for 7–10 days of culture. Cells were fixed and immunolabeled as described above. For detailed information, see supplemental experimental procedures.

Fluorescence imaging, quantification, and statistics

Imaging was carried out with an Apotome system (Carl Zeiss) equipped with the Zen software. Images were processed using Adobe Photoshop (Adobe Systems). All quantifications were conducted using the Fiji software and statistics with GraphPad Prism 6 software. *In vitro* data were deduced from 3-4 experiments performed in duplicates, as detailed in the supplemental information.

SUPPLEMENTAL INFORMATION

Supplemental information can be found online at https://doi.org/10.1016/j.stemcr.2022.10.002.

AUTHOR CONTRIBUTIONS

Conception and design, collection and assembly of data, data analysis and interpretation, and manuscript writing, M.M.; conception and design, collection and assembly of data, and data analysis and interpretation, M.V.; collection and assembly of electron microscopy data and data analysis and interpretation, C.B.; collection and assembly of *in vitro* data and data analysis, C.D.; collection and assembly of immunohistology data, J.C.; data assembly and analysis and manuscript editing and writing, B.G.-D.; conception and design, financial support, administrative support, data analysis and interpretation, manuscript writing, and final approval of the manuscript, A.B.-V.E.

ACKNOWLEDGMENTS

We acknowledge the genotyping (PFGS), cellular imaging (ICM-QUANT), histology (HISTOMICS), cell Culture (CELIS), and animal (PHENOPARC) facilities of ICM for technical assistance. We thank Grigori Enikolopov and Pierre Chambon for generously providing Nestin-GFP, Nestin-CFP, and NestinCreER^{T2}mice. We thank V. Zujovic for helpful experimental advice and comments on the manuscript. This work was supported by the Institut National de la Santé (INSERM), European Leukodystrophy Foundation (ELA; ELA 2010-003C5), the French Multiple Sclerosis Foundation (ARSEP), the National Multiple Sclerosis Society (NMSS; RG 5088-A-1), and the program "Investissements d'Avenir" (ANR-10-IAIHU-06 and ANR-11-INBS-0011–NeurATRIS). M.M. was supported by ELA, ARSEP, and NMSS.

CONFLICT OF INTERESTS

The authors declare no competing interests.

Received: October 1, 2021
Revised: October 3, 2022
Accepted: October 4, 2022
Published: November 8, 2022

REFERENCES

Britsch, S., Goerich, D.E., Riethmacher, D., Peirano, R.I., Rossner, M., Nave, K.A., Birchmeier, C., and Wegner, M. (2001). The transcription factor Sox10 is a key regulator of peripheral glial development. Genes Dev. *15*, 66–78.

Cherkas, P.S., Huang, T.Y., Pannicke, T., Tal, M., Reichenbach, A., and Hanani, M. (2004). The effect of axotomy on neurons and satellite glial cells in mouse trigeminal ganglion. Pain *110*, 290–298.

Czaja, K., Burns, G.A., and Ritter, R.C. (2008). Capsaicin-induced neuronal death and proliferation of the primary sensory neurons located in the nodose ganglia of adult rats. Neuroscience *154*, 621–630.

Devor, M., and Govrin-Lippmann, R. (1985). Neurogenesis in adult rat dorsal root ganglia. Neurosci. Lett. *61*, 189–194.

Donegan, M., Kernisant, M., Cua, C., Jasmin, L., and Ohara, P.T. (2013). Satellite glial cell proliferation in the trigeminal ganglia after chronic constriction injury of the infraorbital nerve. Glia *61*, 2000–2008.

Encinas, J.M., Vaahtokari, A., and Enikolopov, G. (2006). Fluoxetine targets early progenitor cells in the adult brain. Proc. Natl. Acad. Sci. USA *103*, 8233–8238.

Farel, P.B. (2003). Late differentiation contributes to the apparent increase in sensory neuron number in juvenile rat. Brain Res. Dev. Brain Res. *144*, 91–98.

Gallaher, Z.R., Larios, R.M., Ryu, V., Sprunger, L.K., and Czaja, K. (2010). Recovery of viscerosensory innervation from the dorsal root ganglia of the adult rat following capsaicin-induced injury. J. Comp. Neurol. *518*, 3529–3540.

Gallaher, Z.R., Johnston, S.T., and Czaja, K. (2014). Neural proliferation in the dorsal root ganglia of the adult rat following capsaicin-induced neuronal death. J. Comp. Neurol. *522*, 3295–3307.

Garcia-Diaz, B., Bachelin, C., Coulpier, F., Gerschenfeld, G., Deboux, C., Zujovic, V., Charnay, P., Topilko, P., and Baron-Van Evercooren, A. (2019). Blood vessels guide Schwann cell migration in the adult demyelinated CNS through Eph/ephrin signaling. Acta Neuropathol. *138*, 457–476.

Groves, M.J., Schänzer, A., Simpson, A.J., An, S.F., Kuo, L.T., and Scaravilli, F. (2003). Profile of adult rat sensory neuron loss, apoptosis and replacement after sciatic nerve crush. J. Neurocytol. *32*, 113–122.

Hanani, M. (2005). Satellite glial cells in sensory ganglia: from form to function. Brain Res. Brain Res. Rev. *48*, 457–476.

Hanani, M. (2012). Intercellular communication in sensory ganglia by purinergic receptors and gap junctions: implications for chronic pain. Brain Res. *1487*, 183–191.

Hanani, M., Huang, T.Y., Cherkas, P.S., Ledda, M., and Pannese, E. (2002). Glial cell plasticity in sensory ganglia induced by nerve damage. Neuroscience *114*, 279–283.

Hanani, M., and Spray, D. (2020). Emercing importance of satellite glia in nervous system function and dysfunction. Nat. Rev. Neurosci. *22*, 1–14.

Hirose, T., Tani, T., Shimada, T., Ishizawa, K., Shimada, S., and Sano, T. (2003). Immunohistochemical demonstration of EMA/Glut1-positive perineurial cells and CD34-positive fibroblastic cells in peripheral nerve sheath tumors. Mod. Pathol. *16*, 293–298.

Horner, P.J., Power, A.E., Kempermann, G., Kuhn, H.G., Palmer, T.D., Winkler, J., Thal, L.J., and Gage, F.H. (2000). Proliferation and differentiation of progenitor cells throughout the intact adult rat spinal cord. J. Neurosci. *20*, 2218–2228.

Hu, P., and McLachlan, E.M. (2002). Macrophage and lymphocyte invasion of dorsal root ganglia after peripheral nerve lesions in the rat. Neuroscience *112*, 23–38.

Imayoshi, I., Ohtsuka, T., Metzger, D., Chambon, P., and Kageyama, R. (2006). Temporal regulation of Cre recombinase activity in neural stem cells. Genesis *44*, 233–238.

Jessen, K.R., and Mirsky, R. (2008). Negative regulation of myelination: relevance for development, injury, and demyelinating disease. Glia *56*, 1552–1565.

La Forte, R.A., Melville, S., Chung, K., and Coggeshall, R.E. (1991). Absence of neurogenesis of adult rat dorsal root ganglion cells. Somatosens. Mot. Res. *8*, 3–7.

Laranjeira, C., Sandgren, K., Kessaris, N., Richardson, W., Potocnik, A., Vanden Berghe, P., and Pachnis, V. (2011). Glial cells in the mouse enteric nervous system can undergo neurogenesis in response to injury. J. Clin. Invest. *121*, 3412–3424.

Li, H.-Y., Say, E.H.M., and Zhou, X.-F. (2007). Isolation and characterization of neural crest progenitors from adult dorsal root ganglia. Stem Cell. *25*, 2053–2065.

McKay Hart, A., Brannstrom, T., Wiberg, M., and Terenghi, G. (2002). Primary sensory neurons and satellite cells after peripheral axotomy in the adult rat: time course of cell death and elimination. Exp. Brain Res. *142*, 308–318.

Meletis, K., Barnabé-Heider, F., Carlén, M., Evergren, E., Tomilin, N., Shupliakov, O., and Frisén, J. (2008). Spinal cord injury reveals multilineage differentiation of ependymal cells. PLoS Biol. *6*, e182.

Mignone, J.L., Kukekov, V., Chiang, A.-S., Steindler, D., and Enikolopov, G. (2004). Neural stem and progenitor cells in nestin-GFP transgenic mice. J. Comp. Neurol. *469*, 311–324.

Milosavljević, A., Jančić, J., Mirčić, A., Dožić, A., Boljanović, J., Milisavljević, M., and Ćetković, M. (2021). Morphological and functional characteristics of satellite glial cells in the peripheral nervous system. Folia Morphol. *80*, 745–755.

Mirsky, R., Woodhoo, A., Parkinson, D.B., Arthur-farraj, P., Bhaskaran, A., and Jessen, K.R. (2008). Novel signals controlling embryonic Schwann cell development , myelination and dedifferentiation. J. Peripher. Nerv. Syst. *13*, 122–135.

Müller, M., Leonhard, C., Krauthausen, M., Wacker, K., and Kiefer, R. (2010). On the longevity of resident endoneurial macrophages in the peripheral nervous system: a study of physiological macrophage turnover in bone marrow chimeric mice. J. Peripher. Nerv. Syst. *15*, 357–365.

Nagoshi, N., Shibata, S., Kubota, Y., Nakamura, M., Nagai, Y., Satoh, E., Morikawa, S., Okada, Y., Mabuchi, Y., Katoh, H., et al. (2008). Ontogeny and multipotency of neural crest-derived stem cells in mouse bone marrow, dorsal root ganglia, and whisker pad. Cell Stem Cell *2*, 392–403.

Namaka, M.P., Sawchuk, M., MacDonald, S.C., Jordan, L.M., and Hochman, S. (2001). Neurogenesis in postnatal mouse dorsal root ganglia. Exp. Neurol. *172*, 60–69.

Pannese, E. (1981). The satellite cells of the sensory ganglia. Adv. Anat. Embryol. Cell Biol. *65*, 1–111.

Pierucci, A., and de Oliveira, A.L.R. (2006). Increased sensory neuron apoptotic death 2 weeks after peripheral axotomy in C57BL/6J mice compared to A/J mice. Neurosci. Lett. *396*, 127–131.

Pover, C.M., Barnes, M.C., and Coggeshall, R.E. (1994). Do primary afferent cell numbers change in relation to increasing weight and surface area in adult rats? Somatosens. Mot. Res. *11*, 163–167.

Reynolds, B.A., and Weiss, S. (1992). Generation of neurons and astrocytes from isolated cells of the adult mammalian central nervous system. Science *255*, 1707–1710.

Rezajooi, K., Pavlides, M., Winterbottom, J., Stallcup, W.B., Hamlyn, P.J., Lieberman, A.R., and Anderson, P.N. (2004). NG2 proteoglycan expression in the peripheral nervous system: upregulation following injury and comparison with CNS lesions. Mol. Cell. Neurosci. *25*, 572–584.

Richard, L., Topilko, P., Magy, L., Decouvelaere, A.V., Charnay, P., Funalot, B., and Vallat, J.M. (2012). Endoneurial fibroblast-like cells. J. Neuropathol. Exp. Neurol. *71*, 938–947.

Sabourin, J.C., Ackema, K.B., Ohayon, D., Guichet, P.O., Perrin, F.E., Garces, A., Ripoll, C., Charité, J., Simonneau, L., Kettenmann, H., et al. (2009). A mesenchymal-like ZEB1(+) niche harbors dorsal radial glial fibrillary acidic protein-positive stem cells in the spinal cord. Stem Cell. *27*, 2722–2733.

Schaeffer, V., Meyer, L., Patte-Mensah, C., Eckert, A., and Mensah-Nyagan, A.G. (2010). Sciatic nerve injury induces apoptosis of dorsal root ganglion satellite glial cells and selectively modifies neurosteroidogenesis in sensory neurons. Glia *58*, 169–180.

Sghirlanzoni, A., Pareyson, D., and Lauria, G. (2005). Sensory neuron diseases. Lancet, 349–361.

Singec, I., Knoth, R., Meyer, R.P., Maciaczyk, J., Volk, B., Nikkhah, G., Frotscher, M., and Snyder, E.Y. (2006). Defining the actual sensitivity and specificity of the neurosphere assay in stem cell biology. Nat. Methods *3*, 801–806.

Snippert, H.J., and Clevers, H. (2011). Tracking adult stem cells. EMBO Rep. *12*, 113–122.

Takagi, T., Ishii, K., Shibata, S., Yasuda, A., Sato, M., Nagoshi, N., Saito, H., Okano, H.J., Toyama, Y., Okano, H., et al. (2011). Schwann-spheres derived from injured peripheral nerves in adult mice–their in vitro characterization and therapeutic potential. PLoS One *6*, e21497.

Taupin, P. (2007). BrdU immunohistochemistry for studying adult neurogenesis: paradigms, pitfalls, limitations, and validation. Brain Res. Rev. *53*, 198–214.

Usoskin, D., Furlan, A., Islam, S., Abdo, H., Lönnerberg, P., Lou, D., Hjerling-Leffler, J., Haeggström, J., Kharchenko, O., Kharchenko, P.V., et al. (2015). Unbiased classification of sensory neuron types by large-scale single-cell RNA sequencing. Nat. Neurosci. *18*, 145–153.

Vidal, M., Maniglier, M., Deboux, C., Bachelin, C., Zujovic, V., and Baron-Van Evercooren, A. (2015). Adult DRG stem/progenitor cells generate pericytes in the presence of central nervous system (CNS) developmental cues, and Schwann cells in response to CNS demyelination. Stem Cell. *33*, 2011–2024.

Warwick, R.A., and Hanani, M. (2013). The contribution of satellite glial cells to chemotherapy-induced neuropathic pain. Eur. J. Pain *17*, 571–580.

Stem Cell Reports, Volume *17*

Supplemental Information

Satellite glia of the adult dorsal root ganglia harbor stem cells that yield glia under physiological conditions and neurons in response to injury

Madlyne Maniglier, Marie Vidal, Corinne Bachelin, Cyrille Deboux, Jérémy Chazot, Beatriz Garcia-Diaz, and Anne Baron-Van Evercooren

SUPPLEMENTAL INFORMATION

SUPPLEMENTAL FIGURES AND LEGENDS

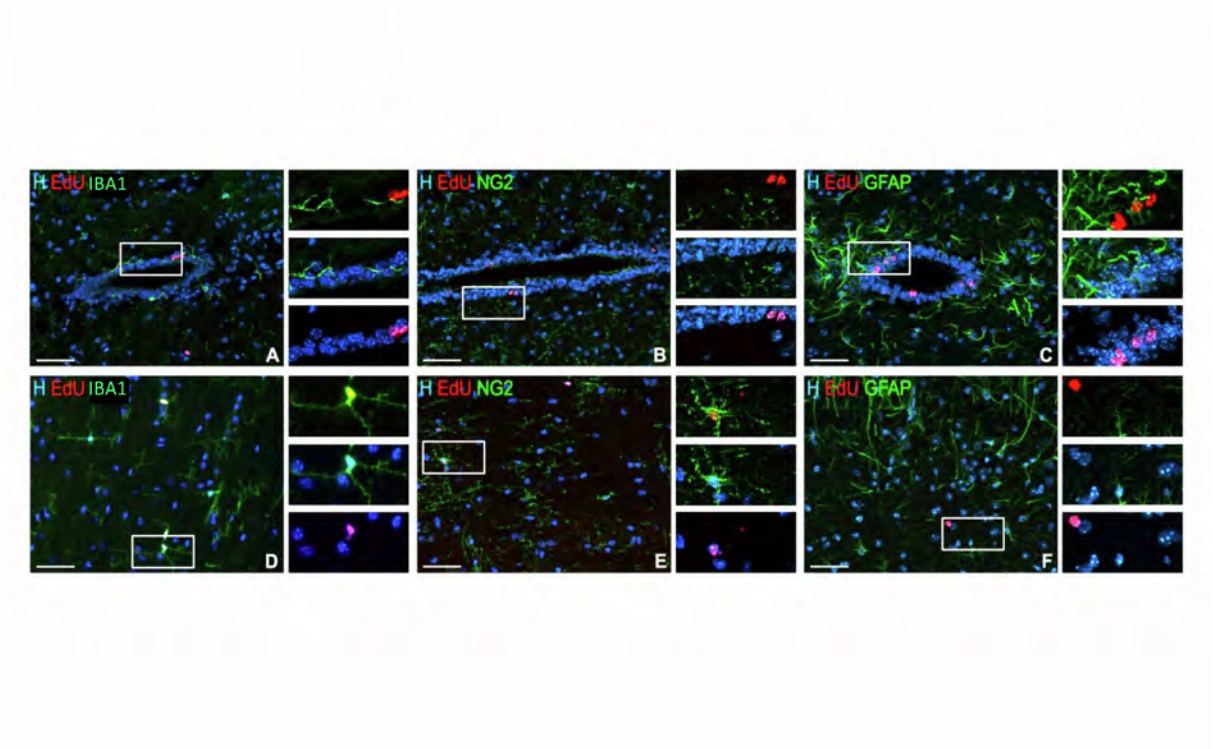

Figure S1 related to Figure 1. ***In Situ characterization of slowly proliferating cells in the adult spinal cord.*** **(A-F)** Double immunohistochemistry for EdU and cell specific markers in the central canal **(A-C)** and parenchyma **(D-F)**. Detection of Iba1+ microglia/macrophages **(A-D)**, NG2+ oligodendrocytes precursors **(B, E)**, GFAP+ glial cells **(C, F)**. Boxed areas are enlarged in right panels. Scale bar: 50 µm.

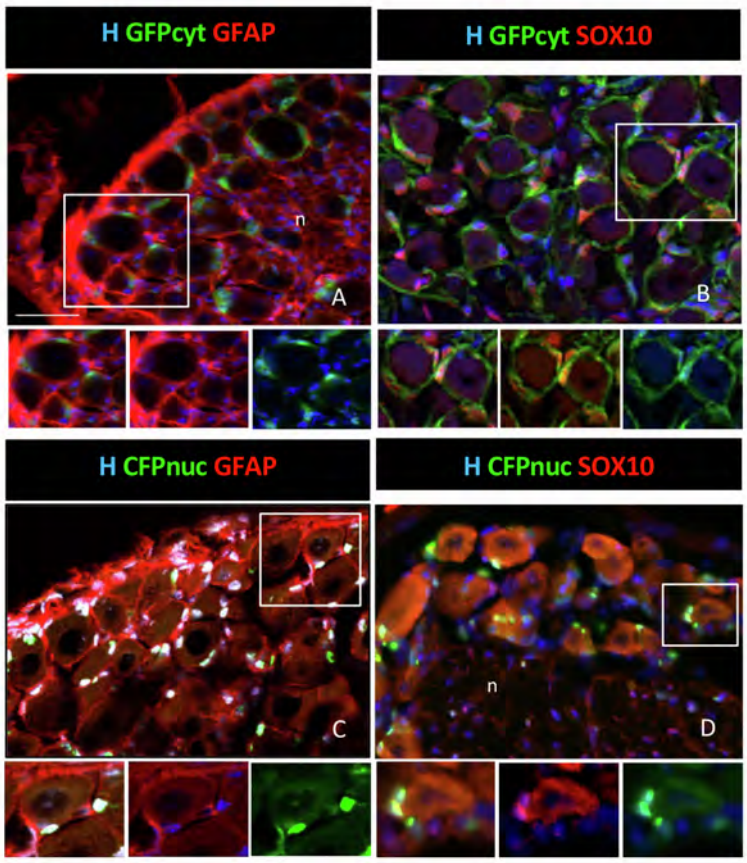

Figure S2 related to Figure 3. **Characterization of DRG-GFPcyt (A, B) and DRG-CFPnuc (C, D) positive cells**. Co-expression with GFAP (**A, C**) or SOX10 (**B, D**). Insets are enlargements of A-D. Scale bar: 50µm

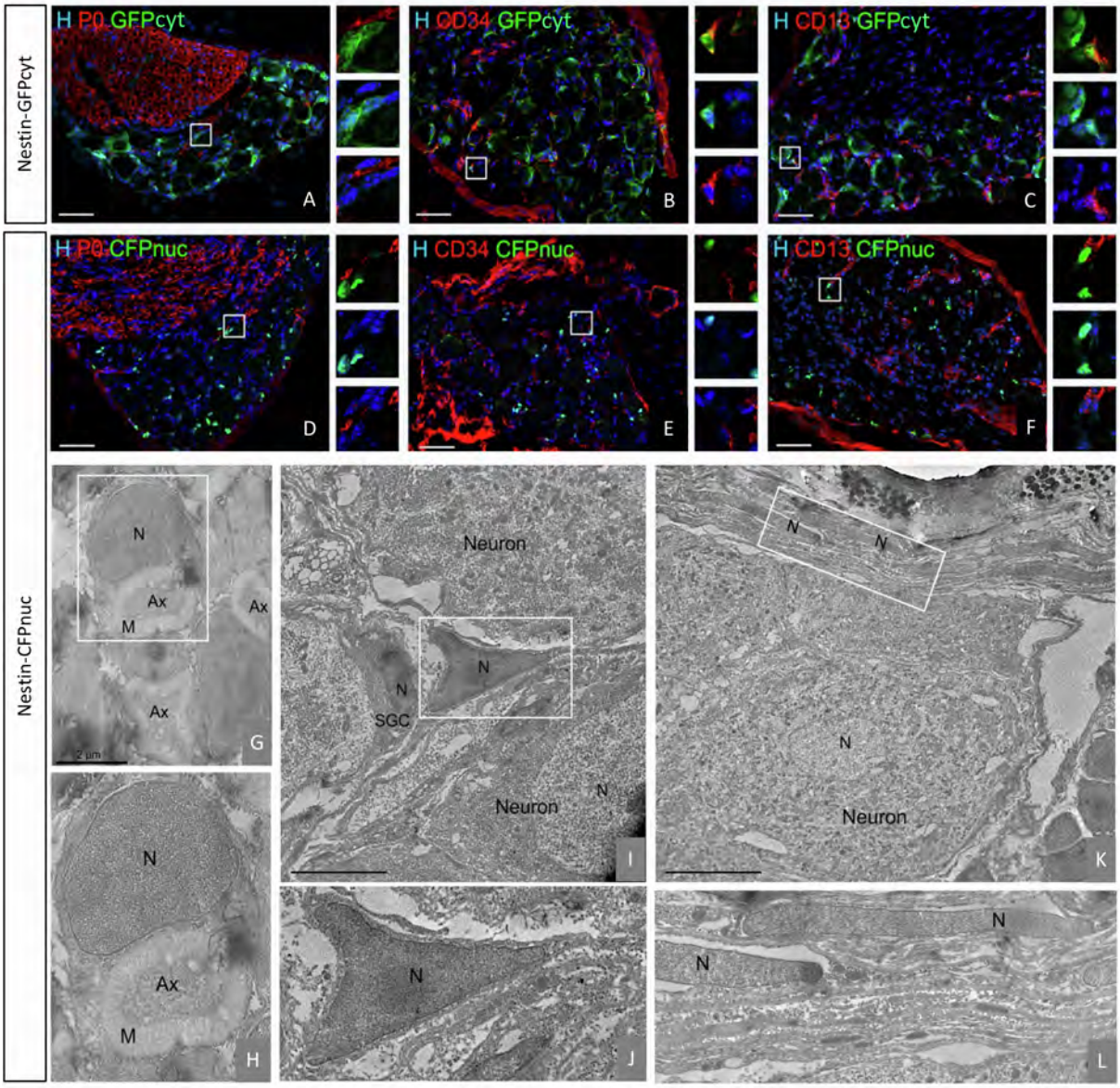

Figure S3 related to Figure 3. ***Characterization of GFPcyt+ or CFPnuc+ cells in the adult DRG of Nestin-GFPcyt and Nestin-CFPnuc reporter mice.*** **(A-F)** Double immunohistochemistry for GFPcyt **(A-C)** or CFPnuc **(D-F)** and cell specific markers to detect P0+ myelinating Schwann cells **(A, D)**, CD34+ endoneurial fibroblasts and endothelial cells **(B, E)** and CD13+ pericytes **(C, F)**. Boxed areas are enlarged in right panels. **(G-L)** Electron microscopy analysis of Nestin-CFPnuc DRG after CFP immunogold labeling. Immunogold particles are never detected in myelinating Schwann cells **(G, H)**, macrophage-like cell **(I, J)** and perineurial fibroblast nuclei **(K, L)**. Lower panels are enlargements of top panels. Scale bar: **A-F**, 50 µm; **G,** 2µm; **I, K,** 5µm**.** A: Axon, M: Myelin, N: Nucleus, SGC: Satellite cell.

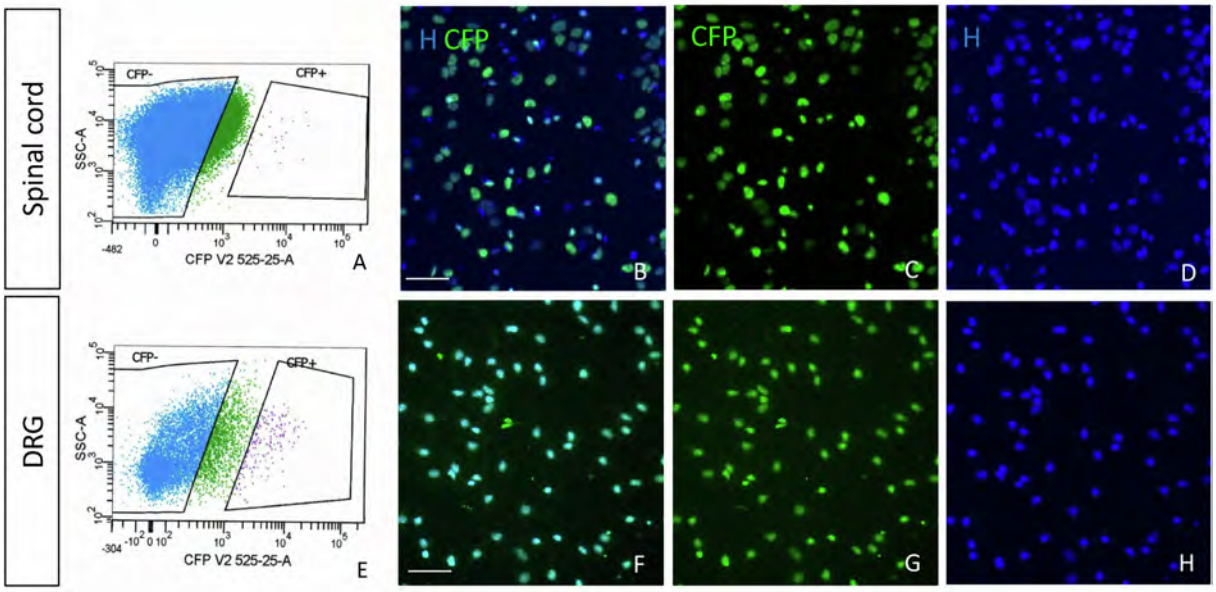

Figure S4 related to Figure 4. ***FACS purification of CFPnuc expressing cells of the spinal cord and DRG***. (**A, E)** FACS gating of CFP+ cells. After sorting cells were allowed to adhere a few hours and were imaged for CFP and Hoechst: (**B, F**) Hoechst and CFP overlay, (**C, G**) CFP expression, (**D, H**) Hoechst expression. Based on Hoechst+ nuclei, around 98% of cells expressed CFP. Scale bar: **B, C, D, F, G, H**, 100µm.

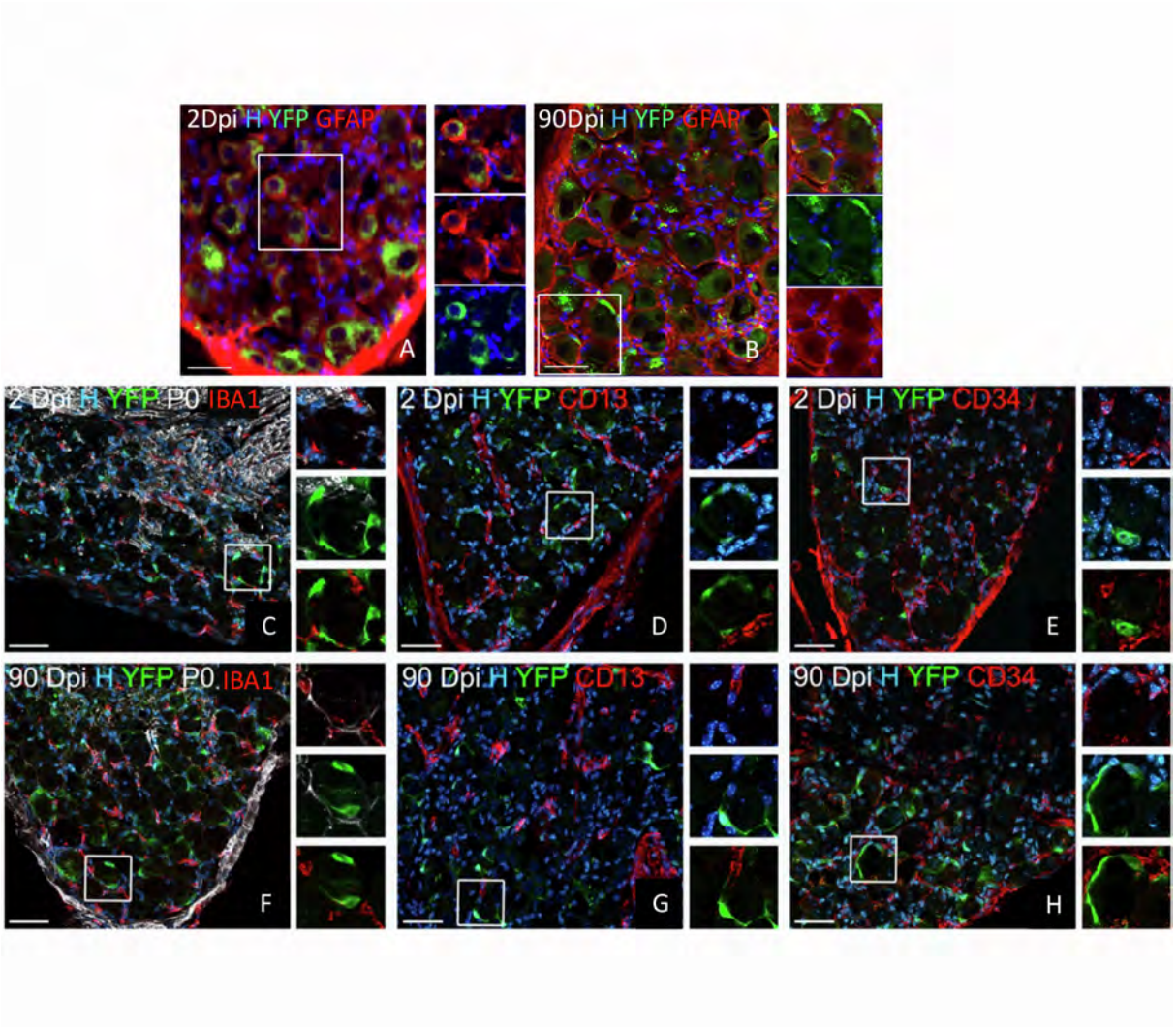

Figure S5 related to Figure 5. ***Characterization of DRG-NSC in non-injured adult Nestin-CreER^{T2}/Rosa26-YFP mice.*** Immunohistochemistry for YFP and cell specific markers to detect co-expression of YFP with **(A, B)** GFAP+ SGC, **(C, F)** P0+ myelinating Schwann cells and Iba1+ microglia/macrophages, **(D, G)** CD13+ pericytes, **(E, H)** CD34+ endoneurial fibroblasts and endothelial cells at 2- and 90 Dpi. Boxed area for each marker is enlarged in the right panel. Scale bar: **A-H**: 50 µm.

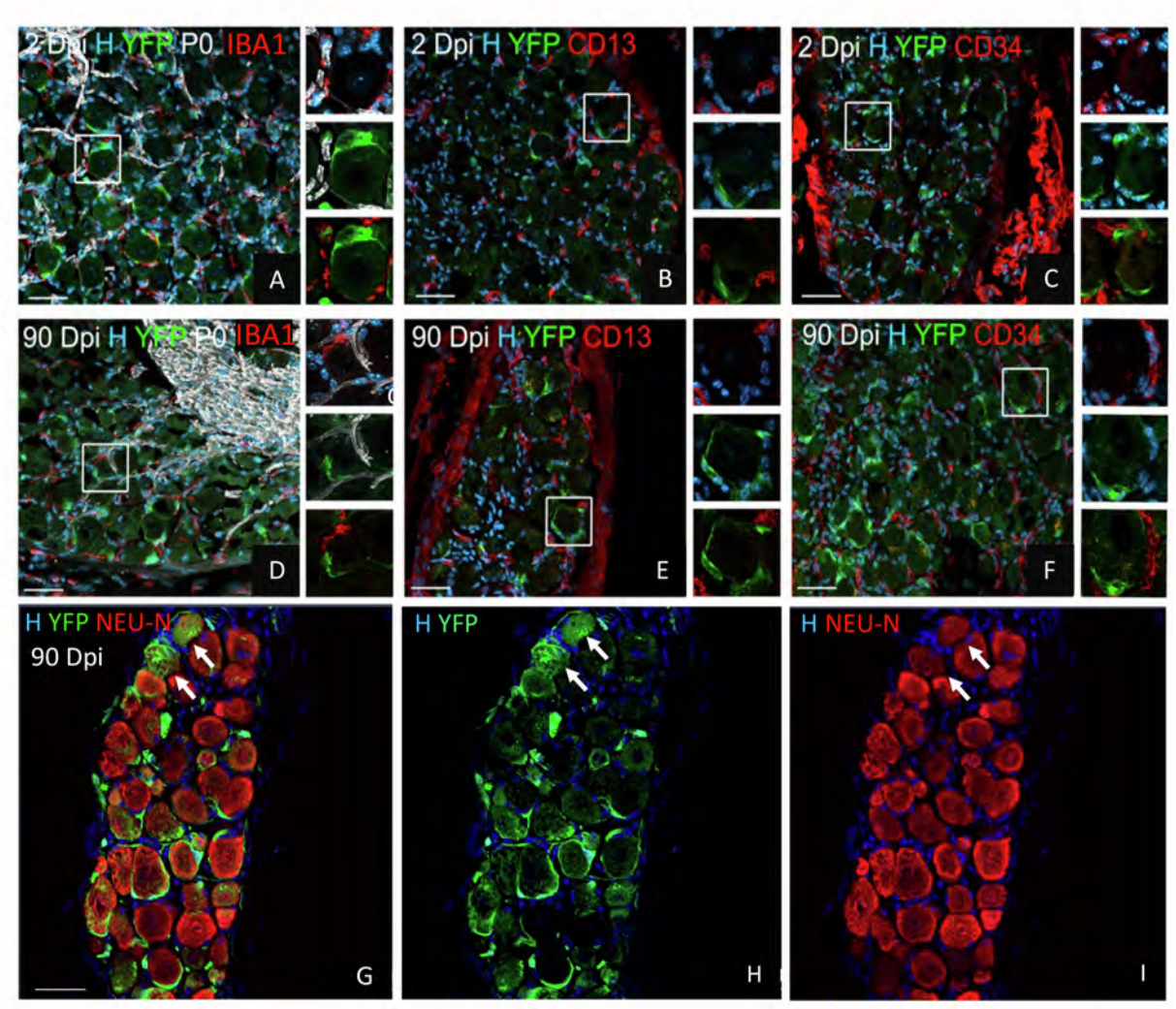

Figure S6 related to Figure 7. ***Characterization of DRG-NSC in injured adult Nestin-CreER^{T2}/Rosa26-YFP mice.*** Immunohistochemistry for YFP and cell type markers to identify Iba1+ microglia/macrophages and P0+ myelinating Schwann cells **(A, D)**, CD13+ pericytes **(B, E)**, and CD34+ endoneurial fibroblasts and endothelial cells **(C, F)** at 2- and 90 Dpi, and YFP+/NEU-N+ neurons at 90Dpi (**G-I**). Boxed area for each marker is enlarged in the right panel. Scale bars: **A-I**: 50µm.

Table S1. List of marker cell specificity for each cell type.

Cell marker	Cell types
IBA1: ionized calcium binding adaptor molecule 1	microglia [1] macrophages[2]
GFAP: glial fibrillary acidic protein	astrocytes[3] stem cells[4] perineuronal satellite glial cells[5]
NG2 glycoprotein	oligodendroglial precursor cells[6] pericytes[7] perineuronal satellite glial cells[8, 9]
SOX10 transcription factor	neural crest cells and their derived progeny including SGC[10, 11]
PV25 parvalbumin	neuronal marker[12, 13]
CD34 transmembrane phospho-glycoprotein protein	endoneurial fibroblasts[14] endothelial cells[15]
CD13 aminopeptidase N	pericytes[16,17]
P0 myelin protein zero	myelinating Schwann cells[18, 19]
CNPase 2′,3′-cyclic nucleotide-3′-phosphodiesterase	oligodendrocytes[20, 21]
MAP2-5 microtubule associated protein 2 and 5	neurons[22, 23]
SMA smooth muscle actin	myofibroblasts[24, 25]
NEU-N Fox-3, Rbfox3, or Hexaribonucleotide Binding Protein-3	neurons[26, 27]
CASPASE 3	apoptotic cells[28, 29]

SUPPLEMENTAL EXPERIMENTAL PROCEDURES

Animals
Nestin CFP-nuclear, Nestin-GFP cytoplasmic, Nestin Cre ERT2, Rosa26-YFP lines were bred and housed under standard conditions of 12-hour light/ 12-hour dark cycles with ad libitum access to dry food and water cycle at ICM pathogen free animal facility. Male and females were included. Experiments were performed according to European Community regulations and INSERM ethical committee (authorization 75-348; 20/04/2005) and were approved by the local Darwin ethical committee.

Sciatic nerve axotomy.
After a resting period of 10 days, tamoxifen-induced animals were anesthetized (Ketamine (100mg/kg) and Xylazin (10mg/kg, Rompun Bayer). In half of the group, the right sciatic nerve was exposed in mid-thigh and cut. A nerve segment of 2 mm was removed to prevent rapid sciatic nerve regeneration. The skin was sutured and mice received two doses of buprenorphin (0.05 mg/kg) in 24 hours. To establish a time course of lesion and re-generation, injured or non-injured induced mice (n= 3-5 per time-point and per group) were sacrificed 2, 14, 30, 60, 90 days dpi. Spinal cord, DRG and sciatic nerves were surgically removed together, in one piece to unambiguously identify the injured DRG (L3-L4-L5), and were processed for immunohistochemistry.

Tissue processing for fluorescent immunohistochemistry.
Four months-old Nestin-CFPnuc and Nestin-GFP-cyt mice (n= 3-4 per line and experimental group) were sacrificed by over-anesthesia (Ketamin-Rompan) and perfused trans-cardially with a solution of 4% paraformaldehyde (PFA) in phosphate saline buffer (PBS) 1X. DRGs, sciatic nerves and spinal cords were post-fixed for one hour in the same fixative, cryo-protected overnight with sucrose 20% in PBS 1X, embedded in Cryomatrix, and frozen in isopentane cooled by liquid nitrogen. Tissues were coronally or horizontally sectioned at 12µm thickness with a cryostat (CM3050S; Leica).

For immunohistochemistry, tissue sections were pre-treated with 0,1 M Glycine for 10 min when needed, followed by incubation in washing buffer (4% bovine serum albumin, BSA) in PBS 1X containing 0.25% Triton) with the following primary antibodies: Chicken anti-GFP (1/300, Aves GFP-1020), mouse anti-NESTIN (1/100, Millipore MAB377), mouse or rabbit anti-GFAP (1/500, Millipore MAB3402 or Dako Z0334), mouse anti-MAP2 (1/200, Sigma M1406), mouse anti-MAP5 (1/200, Sigma M4528, mouse anti-SMA (1/200, Sigma A2547), rabbit anti-NG2 (1/100, Chemicon AB5320), rabbit anti-P75 (1/1000, Millipore AB1554), mouse anti-P0 (Hybridoma[30]), rat anti-CD34 (1/100, BD Biosciences 551387), anti-CASPASE3 (1/400, Cell Signaling), goat anti-SOX10 (1/1000, R&D Systems AF2864), mouse anti-NEU-N (1/100, Millipore MAB377), rabbit NF200 (1/200, Sigma N4142), mouse anti-CNPase (1/200, Millipore MAB326), anti-PDGFRa (1:100, Santa Cruz Biotechnology, sc-338), anti-IBA1 (1:200, Wako, 019-19741), anti-CD-13 (1:50, Biorad MCA2183). After 3 hours, samples were washed three times and incubated for 1 hour with the appropriate fluorochrome-coupled secondary antibodies and Hoechst 33342 (Sigma) diluted in 4% BSA in PBS 1X containing 0.25% Triton. After several rinses in buffer, EdU staining was performed using Click-iT EdU imaging kit (C10340, Invitrogen, Carlsbad, CA) as described in the supplier's protocol. Briefly, slides were incubated with a Click-iT reaction cocktail containing Alexa Fluor 647 azide during 20 min, and washed three times prior mounting in Fluoromount (Sigma). All steps were carried out at room temperature.

Tissue processing for immuno-gold electron microscopy.
Four months-old Nestin-CFP (n=5) mice were sacrificed by overanesthesia (Ketamin-Rompan) and transcardially perfused with 4% PFA in PB 0,1M. DRG and spinal cords were post-fixed one hour in 4% of PFA and 0.3% glutaraldehyde (Sigma-Aldrich). After serial dehydration in a graded ethanol series, tissues were embedded in LRW (Sigma-Aldrich). Post-embedding immunogold was performed incubating ultra-thin sections (80nm) mounted on grids in washing buffer (4% BSA in PB 0.1M) with the primary antibody (chicken anti-GFP antibody, 1/200, Aves GFP-1020). After 1 hour, samples were washed three times and incubated with Goat-anti-Chicken-25nm gold (1/50, Aurion, 125 244). Ultra-thin sections were examined with a HITACHI 120kV HT-7700 transmission electron microscope.

Adult DRG, and spinal cord cultures
Isolation. Transgenic 3 to 4 months-old mice were euthanized by over-anesthesia (CO_2). Spinal cords and DRGs were collected separately into Hank's buffer 1X (HBSS+; Gibco) supplemented with 10%

fetal calf serum (FCS; Gibco) and 1% Penicillin/Streptomycin (P/S; Gibco) and prepared as previously described[31].
Spinal cords were fragmented into 1mm^3 pieces and incubated in DMEM containing 0,05% Trypsin-EDTA (Gibco) and 1% collagenase (Invitrogen) for 30 min at 37°C, then rinsed in stop solution (DMEM plus 10% FCS) and passed through a 40µm cell strainer (BD Biosciences).
DRGs were incubated for 30 min at 37°C, in 0.25% collagenase in DMEM, rinsed in stop solution followed by incubation for 30 min at 37°C, in 0.25% Trypsin. After rinse, DRGs were mechanically dissociated as described above.
Fluorescent Activated Cell Sorting. Cells from the two tissues were purified by FACS, based on their endogenous expression of CFPnuc and GFPcyt (n= 6 independent replicates per transgenic lines).
Expansion. Suspensions of FACS sorted cells were seeded at semi-clonal concentration (<5000 cells/ml) and cultured in suspension as spheres at 37°C/5%CO2 in serum-free medium consisting of DMEM/F12 (1:1; Invitrogen) with B27 and N2 1X (Gibco), 0.8% Insulin (Euromedex), 0,4% glucose, supplemented with epidermal growth factor (EGF, 100ng/mL; Peprotech) and fibroblast growth factor 2 (FGF2, 100ng/mL; Peprotech). Half of the medium was changed every 2-3 days during a period of 10-15 days *in vitro*.
Differentiation. After 15-20 days, spheres were plated on poly-ornithin/laminin (Sigma) coated four well chambers (Greiner) and left in adhesion for 1-2 hours. Adhesive spheres were cultured in the same medium without growth factor for 7-10 days of culture. Cells were fixed in 2% PFA for 10 min prior immunolabeling with the primary and secondary antibodies of interest as described above.

Fluorescence imaging, Quantification and Statistics
Imaging was carried out with an Axio Imager Z2 apotome system (Zeiss) equipped with the Zen software. Images were processed using Adobe Photoshop (Adobe Systems). All quantifications were conducted using the Fiji software. *In vitro* data were deduced from 3-4 experiments performed in duplicates. *In vivo* data were deduced from 5- (for Edu), 10-(for Edu cell type characterization) and 3-(for transgene overlap with other markers) tissue sections from at least 3-4 animals per time-point. Evaluation of EdU expression *in situ* was based on the degree (%) of overlap of EdU- and Hoechst stainings with low <33%, medium <66% and high>66% overlap respectively. Quantification of newly-born neurons (NEU-N+/YFP+) after injury was performed screening 3 DRG- and an average of 700 Neurons- and 625 YFP+ cells/mouse (n=3) and was based on Z stacks images and considering only cells with full overlap of YFP and NEU-N positivities.
Statistical analysis was carried out using GraphPad Prism 6 software. All values were expressed as mean ± SD. Normality in the variable distributions was assessed by the D'Agostino&Pearson omnibus test and Grubbs' test was used to detect and exclude possible outliers. When Normality test was passed, means were compared by two-tailed Student's t test. When one or both groups did not follow a normal distribution, means were compared by two-tailed Mann-Whitney U test. When different independent groups were compared, we performed a one-way or two-way ANOVA plus Dunnett's test or Tukey's multiple comparison tests as specify in each experiment. P-values lower than 0.05 were used as a cut-off for statistical significance.

SUPPLEMENTAL REFERENCES

1. Ohsawa, K., Imai, Y., Sasaki, Y., and Kohsaka, S. (2004). Microglia/macrophage-specific protein Iba1 binds to fimbrin and enhances its actin-bundling activity. J Neurochem *88*, 844-856. 10.1046/j.1471-4159.2003.02213.
2. Kenkhuis, B., Somarakis, A., Kleindouwel, L.R.T., van Roon-Mom, W.M.C., Hollt, T., and van der Weerd, L. (2022). Co-expression patterns of microglia markers Iba1, TMEM119 and P2RY12 in Alzheimer's disease. Neurobiol Dis *167*, 105684. 10.1016/j.nbd.2022.105684
3. Yang, Z., and Wang, K.K. (2015). Glial fibrillary acidic protein: from intermediate filament assembly and gliosis to neurobiomarker. Trends Neurosci *38*, 364-374. 10.1016/j.tins.2015.04.003
4. Liu, Y., Namba, T., Liu, J., Suzuki, R., Shioda, S., and Seki, T. (2010). Glial fibrillary acidic protein-expressing neural progenitors give rise to immature neurons via early intermediate progenitors expressing both glial fibrillary acidic protein and neuronal markers in the adult hippocampus. Neuroscience *166*, 241-251. 10.1016/j.neuroscience.2009.12.026
5. Mohr, K.M., Pallesen, L.T., Richner, M., and Vaegter, C.B. (2021). Discrepancy in the Usage of GFAP as a Marker of Satellite Glial Cell Reactivity. Biomedicines *9*. 10.3390/biomedicines9081022

6. Karram, K., Chatterjee, N., and Trotter, J. (2005). NG2-expressing cells in the nervous system: role of the proteoglycan in migration and glial-neuron interaction. J Anat *207*, 735-744. 10.1111/j.1469-7580.2005.00461.
7. Ozerdem, U., Monosov, E., and Stallcup, W.B. (2002). NG2 proteoglycan expression by pericytes in pathological microvasculature. Microvasc Res *63*, 129-134. 10.1006/mvre.2001.2376
8. Rezajooi, K., Pavlides, M., Winterbottom, J., Stallcup, W.B., Hamlyn, P.J., Lieberman, A.R., and Anderson, P.N. (2004). NG2 proteoglycan expression in the peripheral nervous system: upregulation following injury and comparison with CNS lesions. Mol Cell Neurosci *25*, 572-584. 10.1016/j.mcn.2003.10.009
9. Huang, B., Zdora, I., de Buhr, N., Lehmbecker, A., Baumgartner, W., and Leitzen, E. (2021). Phenotypical peculiarities and species-specific differences of canine and murine satellite glial cells of spinal ganglia. J Cell Mol Med *25*, 6909-6924. 10.1111/jcmm.16701
10. Britsch, S., Goerich, D.E., Riethmacher, D., Peirano, R.I., Rossner, M., Nave, K.A., Birchmeier, C., and Wegner, M. (2001). The transcription factor Sox10 is a key regulator of peripheral glial development. Genes Dev *15*, 66-78. 10.1101/gad.186601
11. Wahlbuhl, M., Reiprich, S., Vogl, M.R., Bosl, M.R., and Wegner, M. (2012). Transcription factor Sox10 orchestrates activity of a neural crest-specific enhancer in the vicinity of its gene. Nucleic Acids Res *40*, 88-101. 10.1093/nar/gkr734
12. Dorst, M.C., Diaz-Moreno, M., Dias, D.O., Guimaraes, E.L., Holl, D., Kalkitsas, J., Silberberg, G., and Goritz, C. (2021). Astrocyte-derived neurons provide excitatory input to the adult striatal circuitry. Proc Natl Acad Sci U S A *118*. 10.1073/pnas.2104119118
13. Filice, F., Vorckel, K.J., Sungur, A.O., Wohr, M., and Schwaller, B. (2016). Reduction in parvalbumin expression not loss of the parvalbumin-expressing GABA interneuron subpopulation in genetic parvalbumin and shank mouse models of autism. Mol Brain *9*, 10. 10.1186/s13041-016-0192-8
14. Hirose, T., Tani, T., Shimada, T., Ishizawa, K., Shimada, S., and Sano, T. (2003). Immunohistochemical demonstration of EMA/Glut1-positive perineurial cells and CD34-positive fibroblastic cells in peripheral nerve sheath tumors. Mod Pathol *16*, 293-298. 10.1097/01.MP.0000062654.83617.B7
15. Richard, L., Topilko, P., Magy, L., Decouvelaere, A.V., Charnay, P., Funalot, B., and Vallat, J.M. (2012). Endoneurial fibroblast-like cells. J Neuropathol Exp Neurol *71*, 938-947. 10.1097/NEN.0b013e318270a941
16. Smyth, L.C.D., Rustenhoven, J., Scotter, E.L., Schweder, P., Faull, R.L.M., Park, T.I.H., and Dragunow, M. (2018). Markers for human brain pericytes and smooth muscle cells. J Chem Neuroanat *92*, 48-60. 10.1016/j.jchemneu.2018.06.001
17. Crouch, E.E., and Doetsch, F. (2018). FACS isolation of endothelial cells and pericytes from mouse brain microregions. Nat Protoc *13*, 738-751. 10.1038/nprot.2017.158
18. Nagarajan, R., Le, N., Mahoney, H., Araki, T., and Milbrandt, J. (2002). Deciphering peripheral nerve myelination by using Schwann cell expression profiling. Proc Natl Acad Sci U S A *99*, 8998-9003. 10.1073/pnas.132080999
19. Jessen, K.R., and Mirsky, R. (2019). Schwann Cell Precursors; Multipotent Glial Cells in Embryonic Nerves. Front Mol Neurosci *12*, 69. 10.3389/fnmol.2019.00069
20. Verrier, J.D., Jackson, T.C., Gillespie, D.G., Janesko-Feldman, K., Bansal, R., Goebbels, S., Nave, K.A., Kochanek, P.M., and Jackson, E.K. (2013). Role of CNPase in the oligodendrocytic extracellular 2',3'-cAMP-adenosine pathway. Glia *61*, 1595-1606. 10.1002/glia.22523
21. Soltani, M.H., Pichardo, R., Song, Z., Sangha, N., Camacho, F., Satyamoorthy, K., Sangueza, O.P., and Setaluri, V. (2005). Microtubule-associated protein 2, a marker of neuronal differentiation, induces mitotic defects, inhibits growth of melanoma cells, and predicts metastatic potential of cutaneous melanoma. Am J Pathol *166*, 1841-1850. 10.1016/S0002-9440(10)62493-5
22. Cheng, A., Krueger, B.K., and Bambrick, L.L. (1999). MAP5 expression in proliferating neuroblasts. Brain Res Dev Brain Res *113*, 107-113. 10.1016/s0165-3806(99)00006-1
23. Hinz, B., Dugina, V., Ballestrem, C., Wehrle-Haller, B., and Chaponnier, C. (2003). Alpha-smooth muscle actin is crucial for focal adhesion maturation in myofibroblasts. Mol Biol Cell *14*, 2508-2519. 10.1091/mbc.e02-11-0729
24. Ina, K., Kitamura, H., Tatsukawa, S., and Fujikura, Y. (2011). Significance of alpha-SMA in myofibroblasts emerging in renal tubulointerstitial fibrosis. Histol Histopathol *26*, 855-866. 10.14670/HH-26.855
25. Wolf, H.K., Buslei, R., Schmidt-Kastner, R., Schmidt-Kastner, P.K., Pietsch, T., Wiestler, O.D., and Blumcke, I. (1996). NeuN: a useful neuronal marker for diagnostic histopathology. J Histochem Cytochem *44*, 1167-1171. 10.1177/44.10.8813082

26. Duan, W., Zhang, Y.P., Hou, Z., Huang, C., Zhu, H., Zhang, C.Q., and Yin, Q. (2016). Novel Insights into NeuN: from Neuronal Marker to Splicing Regulator. Mol Neurobiol *53*, 1637-1647. 10.1007/s12035-015-9122-5
27. Crowley, L.C., and Waterhouse, N.J. (2016). Detecting Cleaved Caspase-3 in Apoptotic Cells by Flow Cytometry. Cold Spring Harb Protoc *2016*. 10.1101/pdb.prot087312
28. Porter, A.G., and Janicke, R.U. (1999). Emerging roles of caspase-3 in apoptosis. Cell Death Differ *6*, 99-104. 10.1038/sj.cdd.4400476
29. Michalski, D., Keck, A.L., Grosche, J., Martens, H., and Hartig, W. (2018). Immunosignals of Oligodendrocyte Markers and Myelin-Associated Proteins Are Critically Affected after Experimental Stroke in Wild-Type and Alzheimer Modeling Mice of Different Ages. Front Cell Neurosci *12*, 23. 10.3389/fncel.2018.00023
30. Yoshimura, T., Satake, M., Kobayashi ,T., (1996) Connexin43 is another gap junction protein in the peripheral nervous system. J Neurochem 1996 Sep;67(3):1252-8
31. Vidal, M., Maniglier, M., Deboux, C., Bachelin, C., Zujovic, V. and Baron-Van Evercooren, A. (2015). Adult DRG stem/progenitor cells generate pericytes in the presence of central nervous system (CNS) developmental cues, and Schwann cells in response to CNS demyelination. *Stem Cells* 33, 2011–24.